Pratham
IIT Bombay Student Satellite

Conceptual Design Report

Power System

Mehul D. Tikekar (Team leader)

Narendra Shiradkar

Ameya Damle

Soham Mehta

Chiraag Juvekar

Mehul Jain

Indian Institute of Technology Bombay

July, 2008

Table of Contents

1. Introduction

This document contains the conceptual design of the electrical power supply of Pratham, IIT Bombay's student satellite. It details the main requirements, design and analysis of the power system of the satellite. It contains results of simulation and actual testing of circuits that was done over the past six months, the inferences drawn from the results and the decisions taken on their basis.

1.1. Requirements of PS

The main requirements placed upon the power supply (*PS*) of the satellite can be stated as follows:

To provide electrical power as per demands of the other subsystems.

To collect data of the health of the power system and send it to the on-board computer (*OBC*) for down linking.

It is a completely autonomous system which collects power from sources, stores it and distributes it to the various electrical loads. Hence, a list of all the functions can be made.

1.2. Functions of PS

1. To collect solar power.
2. To supply power to various electronic circuits as required.
3. To store the excess power available.
4. To monitor condition of each load.
5. To switch off a load if it is malfunctioning or not in use.
6. To store all voltage, current and temperature values indicating the health of the PS and relay this information to the OBC
7. To power-up the satellite upon ejection from the launch vehicle

2. Power Budget

The power budget is a calculation of the total power requirements of the various subsystems and the total power input from various sources.

2.1. Power requirements

The other satellite subsystems and their functions are explained in brief.

Payload (*PAY*) – The satellite mission is to measure the total electron count (*TEC*) in the ionosphere. This is accomplished by sending a linearly polarized radio wave from the satellite to the ground station. In the process, the plane of polarization of the wave rotates by an angle proportional to the amount of free electrons in the medium it traversed through. This angle is measured to give the TEC.

Communication (*COM*) – Responsible for communication between the satellite and ground station. The satellite has a beacon and a communication downlink both of which are utilized by the payload. No uplink has been planned for this satellite.

Attitude determination and control system (*ADCS*) – Controls the orientation of the satellite in space to ensure that the antennae point in a particular direction. The attitude is determined by various sensors like magnetometer, sun-sensors, GPS and rate gyroscopes. Control is achieved using magnetotorquer coils which provide torque depending on the current passing through them.

On-board computer (*OBC*) – Handles information to be transmitted and interfaces with the sensors and actuators for the ADCS.

Structures and thermals (*ST*) – Looks after the proper placement of all components on the satellite to ensure that they are operated in their safe operation conditions.

The power requirements of all the various subsystems are given below.

Loads	Average power	Peak power	Voltage
On-board computer	1W	1W	3.3V
ADCS	2.25W	2.25W	3.3V, 5V and unregulated battery voltage
Beacon	2W	2W	3.3V
Downlink	0.06W	2W	3.3V
Thermals	0.3W	2W	Unregulated battery voltage

2.2. Power sources

The main sources of power for a space mission are solar power, chemical power (non-rechargeable cells, fuel cells) and nuclear power. Chemical power is suitable only for short missions and nuclear power is suitable only for large missions with large power requirements. For small satellites like Pratham, with a designed lifetime of a few months to a few years, solar power is the most suitable source of power. Recent advancements in solar cell technology make it possible to harness Sun's energy with considerable efficiency (around 25%). Newer cells based on Gallium Arsenide (GaAs) have higher efficiencies as compared to Silicon (Si) cells and also degrade slower in the harsh space environment.

2.2.1. Incident radiation

The satellite receives light from three sources: Direct solar radiation, Sunlight reflected from Earth and Earth's thermal radiation.

Direct solar radiation: The intensity of sunlight available near Earth is about 1353 W/m^2. The actual value varies by 6.9% percent through the year but the standard accepted value of the solar constant (*S*) is 1353 W/m^2. The energy distribution of sunlight at the top of the Earth's atmosphere is called the AM0 (air-mass 0) spectrum. For the surface of the Earth, other spectrums AM1 and AM1.5 are used as standards for testing solar cells.

Sunlight reflected from the Earth: The surface of the Earth and the atmosphere reflect the incident sunlight to a significant degree. The ratio of the energy reflected diffusively to the energy incident is called albedo. The albedo of Earth is different at different places; it is close to 1 near the poles whereas it is quite small over oceans. The average value is around 30%.

Earth's thermal radiation: Earth emits light in the infrared region. The intensity of this thermal radiation is about 237 W/m^2 in a low Earth orbit (LEO).

2.2.2. Body mounted solar panels

The satellite is a cuboid with a size of 230mm x 230 mm x 230mm. One of the faces is required to be pointing to the Earth at all times for communication. Another face is required to be in the direction of motion of the satellite for the payload. Solar panels are present on all faces except the Earth-facing one (called as the nadir surface).

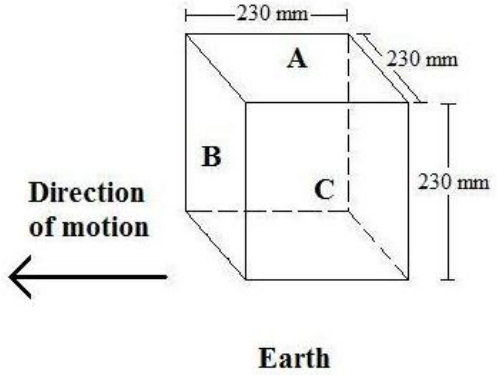

Figure 1: Satellite size

In the accompanying figure, the faces A, B and C are mutually perpendicular. The faces opposite to them are named as A',B' and C' respectively. A' is the nadir surface and A is the zenith surface. The satellite moves in the direction along the outward normal to B.

Since the antennae are oriented with a slight angle towards the Earth, they do not obstruct the path of direct sunlight falling on the solar panels. Hence, a shadow

analysis is not required for the direct solar radiation.

The total useful power on each of the faces is found to be:

A	A'	B	B'	C	C'	Total
21W	7W	17W	17W	20W	2W	84W

The calculation of these numbers is detailed below.

2.2.3. Direct solar power calculation

The satellite is to be placed in a 10.30 am Sun-synchronous orbit with a 98° inclination at an altitude of 670 km. The radius of the satellite orbit is thus, R = 7070km. The time period of the orbit is T = 5916 sec (98.6 minutes). Hence, the satellite's angular velocity of rotation about the Earth is $\omega = 0.00106$ rad/sec.

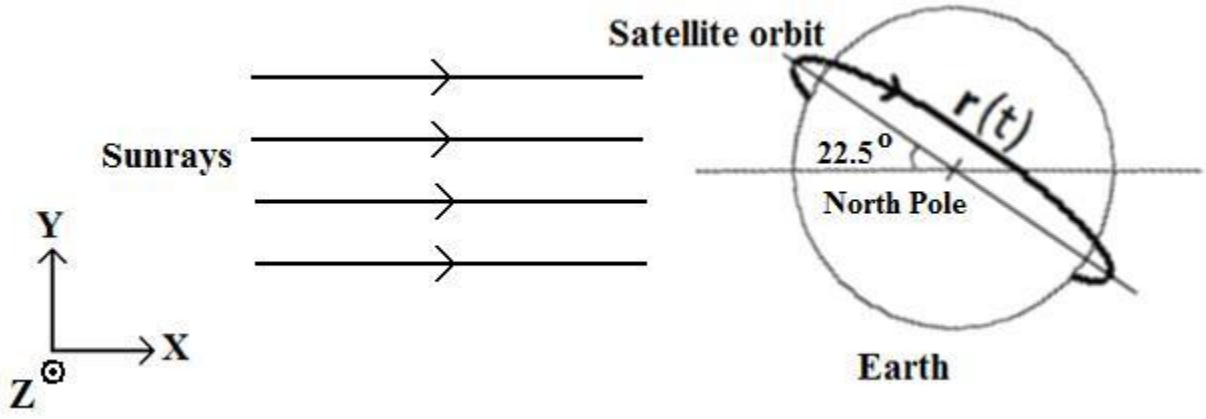

Figure 2: Satellite orbit

In the above diagram, Earth is taken as the origin for the coordinate system. The position of the satellite as a function of time, starting with the point just above the North Pole is

$$\therefore \vec{r}(t) = R\begin{bmatrix} \cos\lambda & \sin\lambda & 0 \\ -\sin\lambda & \cos\lambda & 0 \\ 0 & 0 & 1 \end{bmatrix}\begin{bmatrix} \sin(\omega t) \\ \cos(\omega t)\sin 8° \\ \cos(\omega t)\cos 8° \end{bmatrix} = R\begin{bmatrix} \cos\lambda\sin(\omega t)+\sin\lambda\cos(\omega t)\sin 8° \\ -\sin\lambda\sin(\omega t)+\cos\lambda\cos(\omega t)\sin 8° \\ \cos(\omega t)\cos 8° \end{bmatrix}$$

Hence, the velocity of the satellite is

$$\therefore \vec{v}(t) = R\omega\begin{bmatrix} \cos\lambda\cos(\omega t)-\sin\lambda\sin(\omega t)\sin 8° \\ -\sin\lambda\cos(\omega t)-\cos\lambda\sin(\omega t)\sin 8° \\ -\sin(\omega t)\cos 8° \end{bmatrix}$$

Thus, the normals to the three faces A, B and C are found to be

$$\hat{n}_1(t) = \begin{bmatrix} \cos\lambda \sin(\omega t) + \sin\lambda \cos(\omega t)\sin 8° \\ -\sin\lambda \sin(\omega t) + \cos\lambda \cos(\omega t)\sin 8° \\ \cos(\omega t)\cos 8° \end{bmatrix}$$

$$\hat{n}_2(t) = \begin{bmatrix} \cos\lambda \cos(\omega t) - \sin\lambda \sin(\omega t)\sin 8° \\ -\sin\lambda \cos(\omega t) - \cos\lambda \sin(\omega t)\sin 8° \\ -\sin(\omega t)\cos 8° \end{bmatrix}$$

$$\hat{n}_3(t) = \hat{n}_1(t) \times \hat{n}_2(t)$$

From this, the angle of incidence of sunlight on the faces A, B and C are found. If the angles are denoted as α, β and γ respectively, then

$$\cos\alpha = -\hat{i} \cdot \hat{n}_1(t) = -\cos\lambda \sin(\omega t) - \sin\lambda \cos(\omega t)\sin 8°$$

$$\cos\beta = -\hat{i} \cdot \hat{n}_2(t) = -\cos\lambda \cos(\omega t) + \sin\lambda \sin(\omega t)\sin 8°$$

$$\cos\gamma = -\hat{i} \cdot \hat{n}_3(t) = -\sin\lambda \cos 8°$$

The intensity of light incident on face A is

$$I_A = S\cos\alpha \text{ when } \cos\alpha > 0 \text{ and } 0 \text{ otherwise}$$

Similarly, for the other faces,

$$I_{A'} = S\cos\alpha \text{ when } \cos\alpha < 0 \text{ and } 0 \text{ otherwise}$$

$$I_B = S\cos\beta \text{ when } \cos\beta > 0 \text{ and } 0 \text{ otherwise}$$

$$I_{B'} = S\cos\beta \text{ when } \cos\beta < 0 \text{ and } 0 \text{ otherwise}$$

$$I_C = S\cos\gamma \text{ when } \cos\gamma > 0 \text{ and } 0 \text{ otherwise}$$

$$I_{C'} = S\cos\gamma \text{ when } \cos\gamma < 0 \text{ and } 0 \text{ otherwise}$$

The averages of I_A, $I_{A'}$, I_B, $I_{B'}$, I_C and $I_{C'}$ over one orbit have to be calculated taking the eclipse region into account.

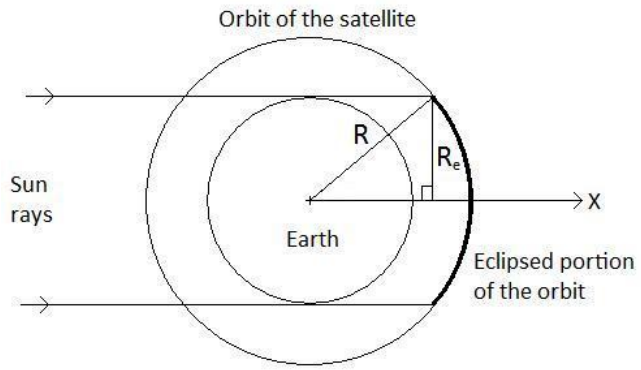

From the adjoining figure, we can see that the satellite enters the eclipsed region when,

$$x > \sqrt{R^2 - R_e^2}$$

$$\Rightarrow R(\cos\lambda\sin(\omega t) + \sin\lambda\cos(\omega t)\sin 8°) > \sqrt{R^2 - R_e^2}$$

$$\Rightarrow 0.925\sin(\omega t + 3.3°) > 0.425$$

$$\Rightarrow \sin(\omega t + 3.3°) > 0.46$$

$$\Rightarrow 27.4° < \omega t + 3.3° < 152.6°$$

$$\Rightarrow 24.1° < \omega t < 149.3°$$

Figure 3: The eclipsed portion of the orbit

The intensities I_1, I_2 and I_3 are now plotted over the period of one orbit and their averages are found.

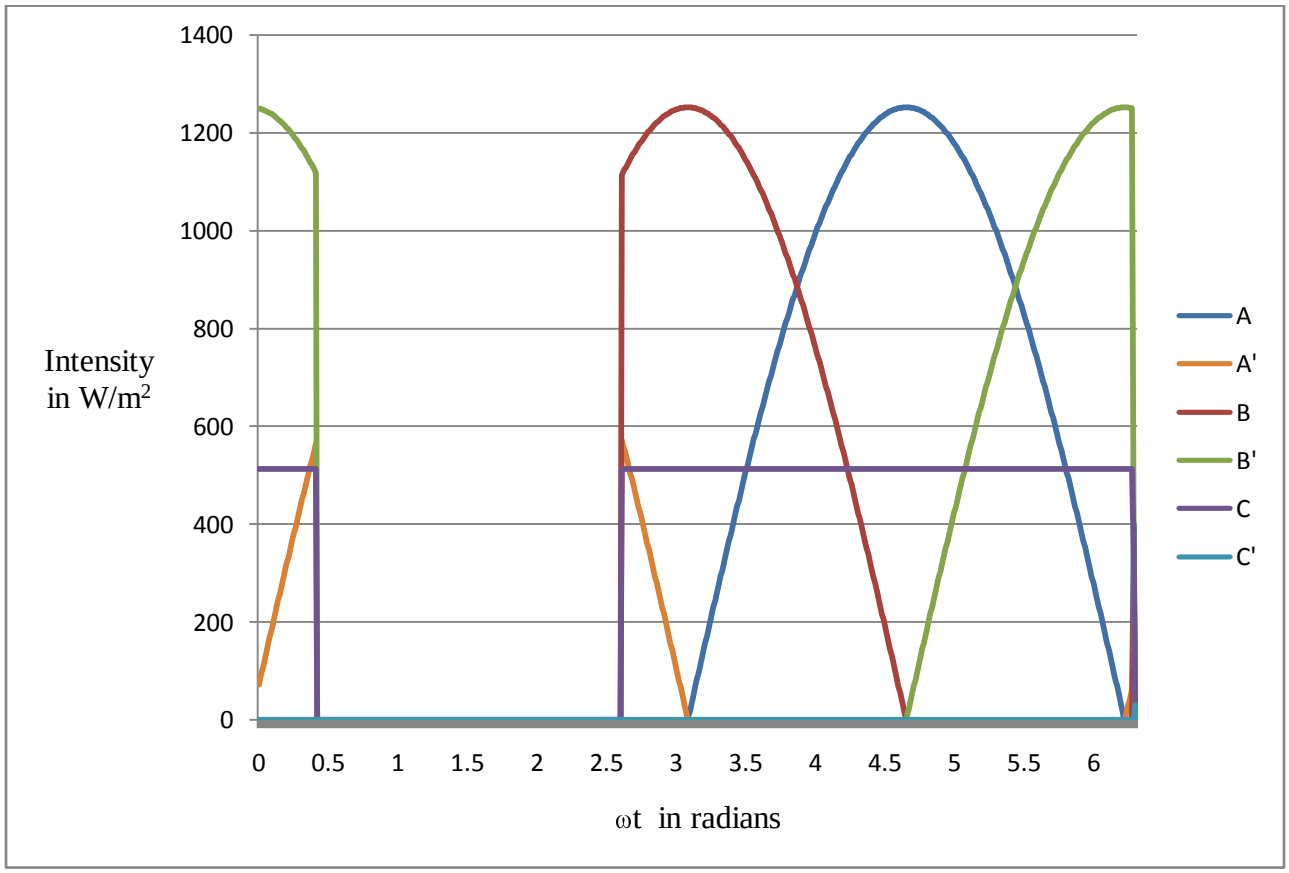

Figure 4: Direct solar intensities over the faces

The average intensities on the faces over one orbit are:

A	A'	B	B'	C	C'
398 W/m^2	44 W/m^2	291 W/m^2	291 W/m^2	334 W/m^2	0 W/m^2

2.2.4 Power due to Earth's albedo

The sunlight reflected off the Earth's surface induces power in solar cells just like direct sunlight. The albedo of an object is the extent to which it diffusely reflects light from the sun. The Earth albedo is conventionally measured as a fraction of the direct incident sunlight; however, here, it will be used to mean the actual intensity of the reflected light. The Earth albedo model used by us was developed by D.N.Bhanderi, Alborg University (www.bhanderi.dk) as a Matlab model. It calculates the amount of Earth albedo arriving at an object in space, maintaining information of direction of the Earth albedo, useful for objects in low Earth-orbit. The directional information is maintained by partitioning the Earth surface in small cells, and calculating the Earth albedo contribution of each cell.

In order to calculate the Earth albedo, the model needs three input parameters in the ECEF (earth centred earth fixed) frame: Satellite position vector, Sun position vector, Earth surface reflectivity. Reflectivity data is available from the TOMS project, NASA (http://toms.gsfc.nasa.gov/reflect). The Total Ozone Mapping Spectrometer, launched in July 1996 onboard an Earth Probe Satellite (TOMS/EP), continues NASA's long term daily mapping of the global distribution of the Earth's atmospheric ozone. TOMS/EP takes high-resolution measurements of the total column amount of ozone from space that began with NASA's Nimbus-7 satellite in 1978 and continued with the TOMS aboard a Russian Meteor-3 satellite till 1994. This NASA-developed instrument measures ozone, aerosol concentration, Earth's reflectivity, etc. In addition to ozone, TOMS measures sulphur-dioxide released in volcanic eruptions. The U.S. Federal Aviation Administration (FAA) is studying ways to use these measurements to detect volcanic ash clouds that are hazardous to commercial aviation.

Matlab converted data and pre-processed data are available within the Earth Albedo Toolbox, which also includes Matlab functions for loading TOMS data into Matlab manually. The resolution of the TOMS data is 180 x 288 data points. That is 51,840 cells of 1 deg latitude and 1.25 deg longitude. This resolution may be decreased in the toolbox software. The figure alongside shows the plot of the 2004 annual mean of the TOMS reflectivity data as a percentage of the direct solar radiation intensity (=1353 W/m^2).

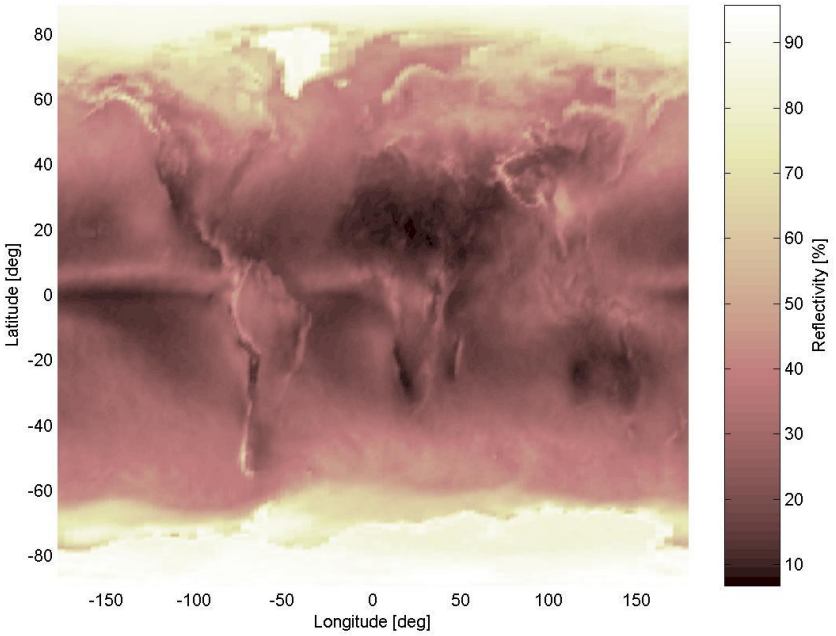

Figure 5: TOMS reflectivity data for 2004

The mathematical model (MATLAB toolbox):

The model calculates the Earth albedo from each data point in the reflectivity data. The grid point (θ, ϕ) defines the longitude and lattitude of the data point. This point defines a cell with an area $A(\phi)$ expanded by 1 deg latttitude and 1.25 deg longitude. The incident irradiance E_0 arrives from the direction $\hat{r}_{sun}$ to the Sun, the angle of which is defined from the cell normal $\hat{n}_c$. The incident irradiance is assumed to be constant for all cells. The direction of the satellite is defined by $\hat{r}_{sat}$, also defined by an angle to the cell normal. The reflected irradiance at satellite distance from the cell centre is denoted $E_c(\theta, \phi)$.

Figure 6 below shows all these parameters.

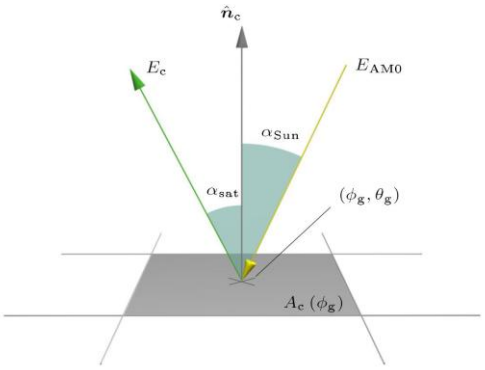

Figure 6: Parameters for an Earth area cell

$\rho(\theta, \phi)$ is the mean reflectivity of the cell as obtained from the database, which contains per-cell reflectivity for each day of the years 2000-2005 (we are currently using the data for a fixed date only). Given the above definitions, a matrix of contributions from each cell in the input data is calculated. The contribution for each cell is given by

$$E_c(\theta, \phi) = \frac{\rho(\theta, \phi) E_0 A(\phi)(\hat{r}_{sun} \,.\, \hat{n}_c)(\hat{r}_{sat} . \hat{n}_c)}{\pi |\hat{r}_{sat}|^2} \quad \text{for cells which are sunlit}$$

$$= 0 \qquad \text{otherwise}$$

Calculating the contribution to the power output from each cell is done by the "Earth Albedo Simulation block". The "Perpendicular Equivalent" block incorporates the effect of all the area cells assuming a simple cosine dependency of output current on the angle of incidence. All these Simulink blocks are used in the following Simulink model.

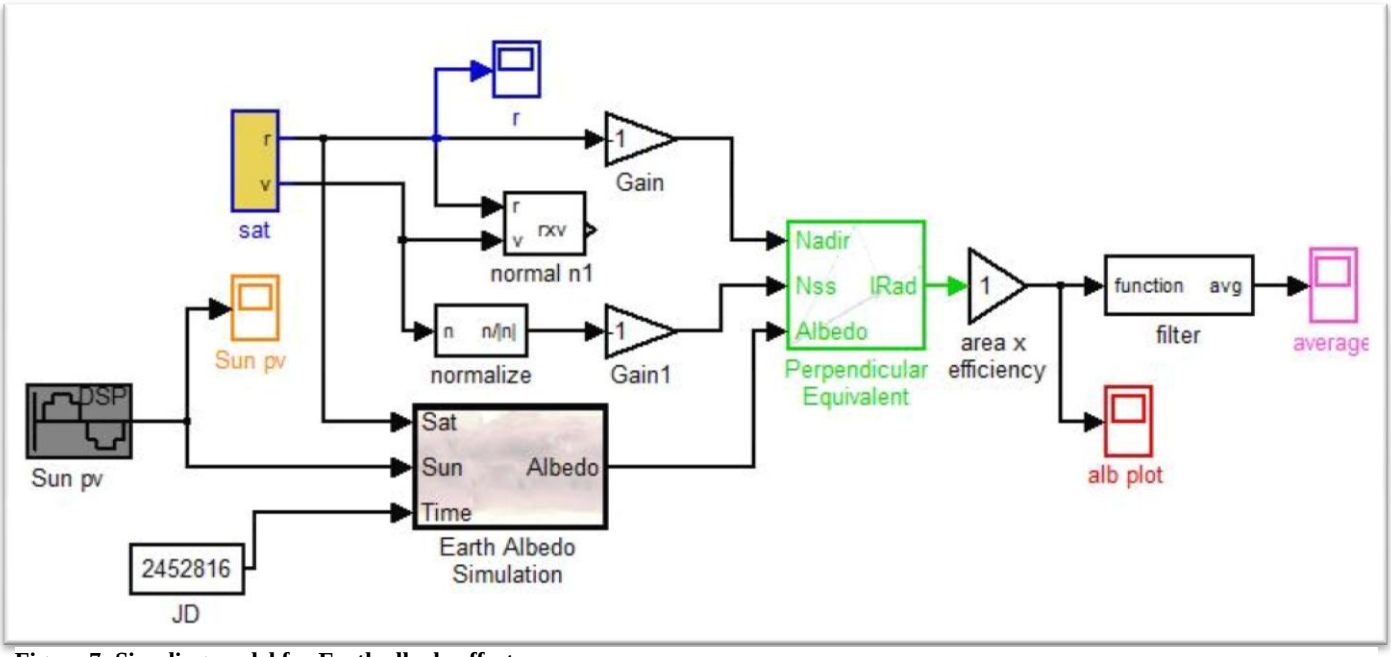

Figure 7: Simuling model for Earth albedo effect

Description of the simulink model:

The 'earth albedo simulation' and 'perpendicular equivalent' are the main blocks which calculate the albedo, using previous year's reflectivity data given the position of the satellite and the sun in the ECEF frame. This frame is shown in figure 4. The reflectivity data is taken for the day indicated by the bottom left block, the Julian Date. The JD 2452816 in the figure corresponds to 25th of June, 2003.

The grey block on the bottom left gives the sun's co-ordinates in the same frame, this is simply $x = 1.5\,AU \sin \omega t\,, y = 0, z = 1.5\,AU \cos \omega t$. We have neglected the earth's revolution i.e. the sun's motion is taken to be in a fixed plane. This is justified since the satellite's life is of the order of 4 months and we are looking only at daily, not annual variations. The yellow block "sat" gives the satellites position and velocity vectors. The construction of the 'sat' block is shown below.

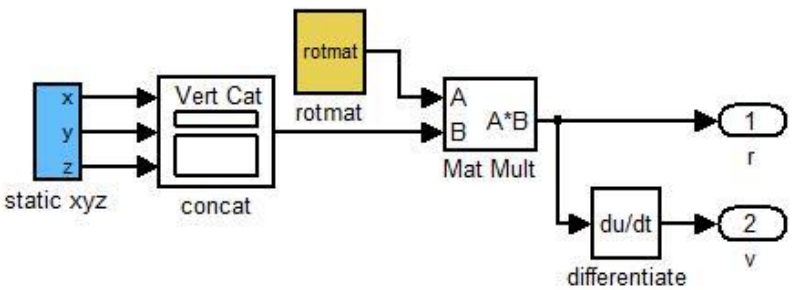

Figure 8: The "sat" block

The ‘static xyz’ block gives the position in an Earth centered (but not fixed) frame as below.

$$\vec{r}(t) = R\begin{bmatrix} \cos\lambda & \sin\lambda & 0 \\ -\sin\lambda & \cos\lambda & 0 \\ 0 & 0 & 1 \end{bmatrix}\begin{bmatrix} \sin(\omega t) \\ \cos(\omega t)\sin 8^\circ \\ \cos(\omega t)\cos 8^\circ \end{bmatrix} = R\begin{bmatrix} \cos\lambda\sin(\omega t) + \sin\lambda\cos(\omega t)\sin 8^\circ \\ -\sin\lambda\sin(\omega t) + \cos\lambda\cos(\omega t)\sin 8^\circ \\ \cos(\omega t)\cos 8^\circ \end{bmatrix}$$

Here $\lambda = 22.5^0$ and $R = 7070\ km$ are orbit parameters.

This is multiplied by the corresponding y-rotation matrix (rotmat) to obtain the position in the ECEF frame.

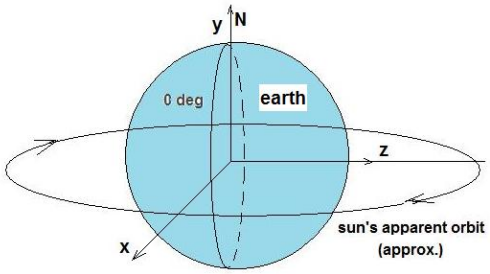

Figure 9: The ECEF frame

$$\text{rotmat} = \begin{pmatrix} \cos(\omega_1 t) & 0 & \sin(\omega_1 t) \\ 0 & 1 & 0 \\ -\sin(\omega_1 t) & 0 & \cos(\omega_1 t) \end{pmatrix}$$

Here, ω_1 is the angular rate of rotation of the Earth.

The last block computes the average as $< f > = \int_0^t f\ dt / \int_0^t dt$.

Lastly, the ‘area x efficiency’ gain was used so that we could plot directly the generated power as required (currently it is set to 1).

The perpendicular equivalent of the albedo (in W/m^2 on Y axis) plotted for 8.64x10^4 sec (i.e. 1 day which is about 14 orbits) on the five faces C, C’, B, B’ and A’ are shown below.

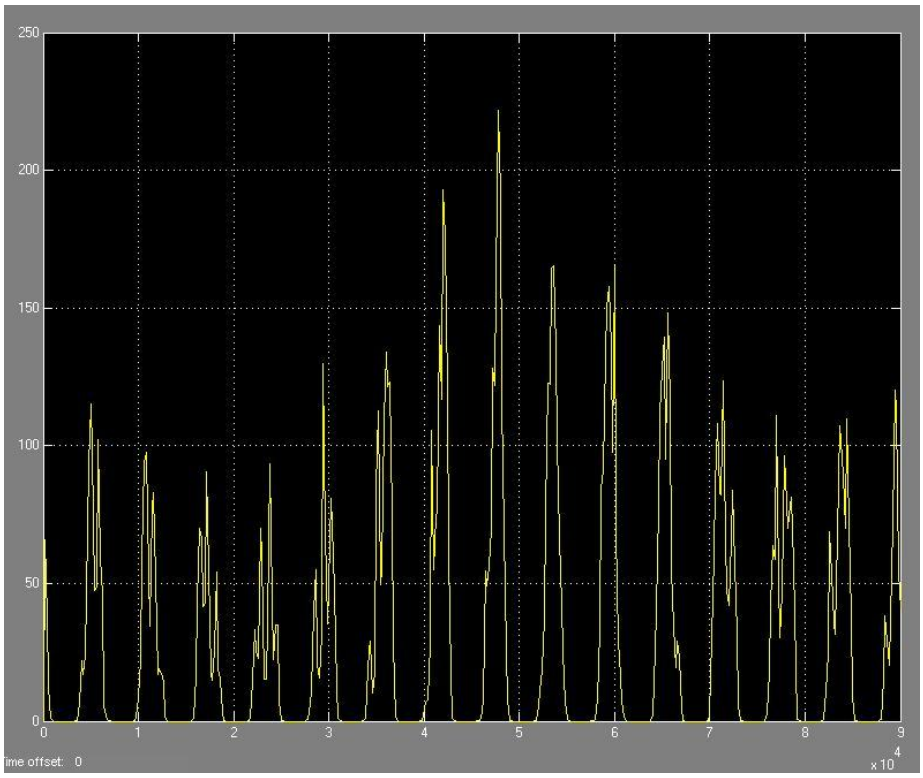

Figure 10: Albedo on the face C

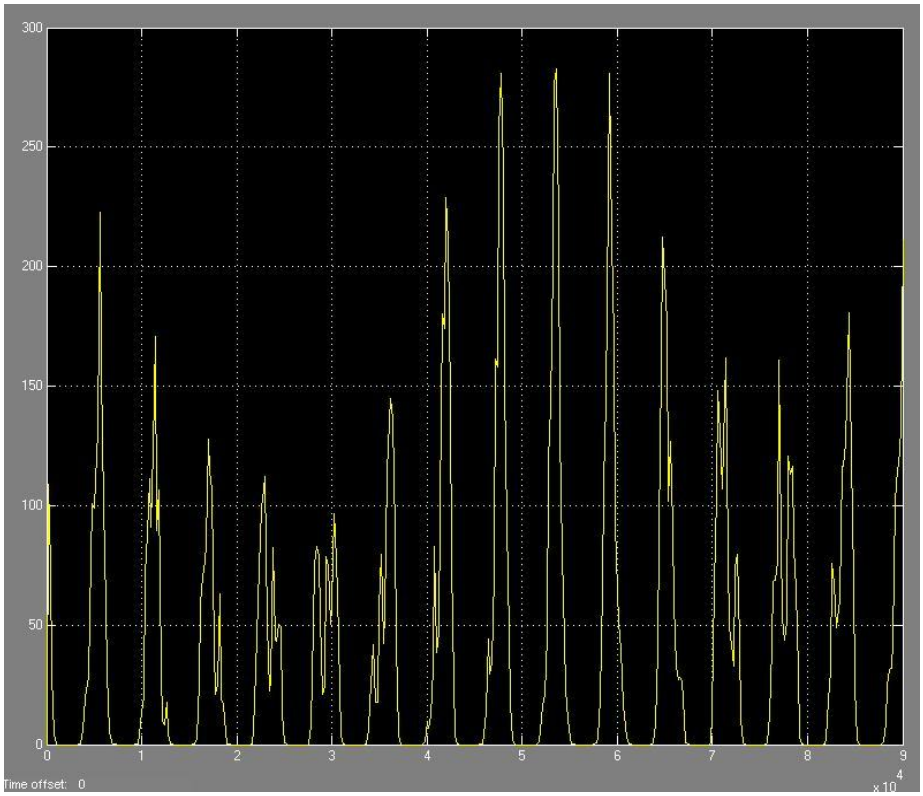

Figure 11: Albedo on the face C'

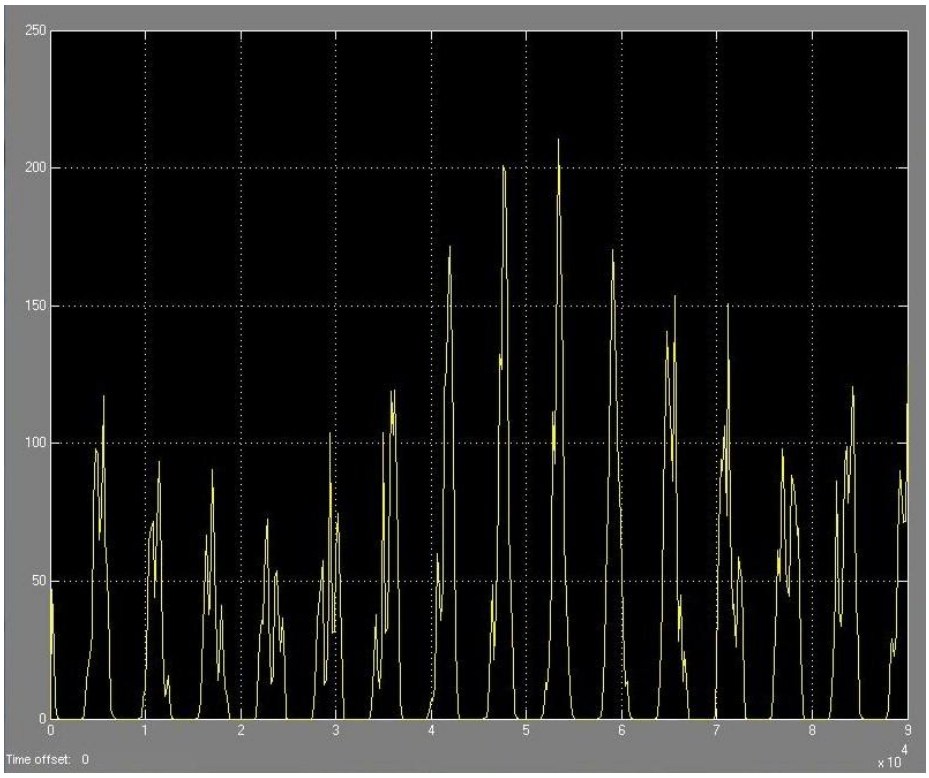

Figure 12: Albedo on the face B

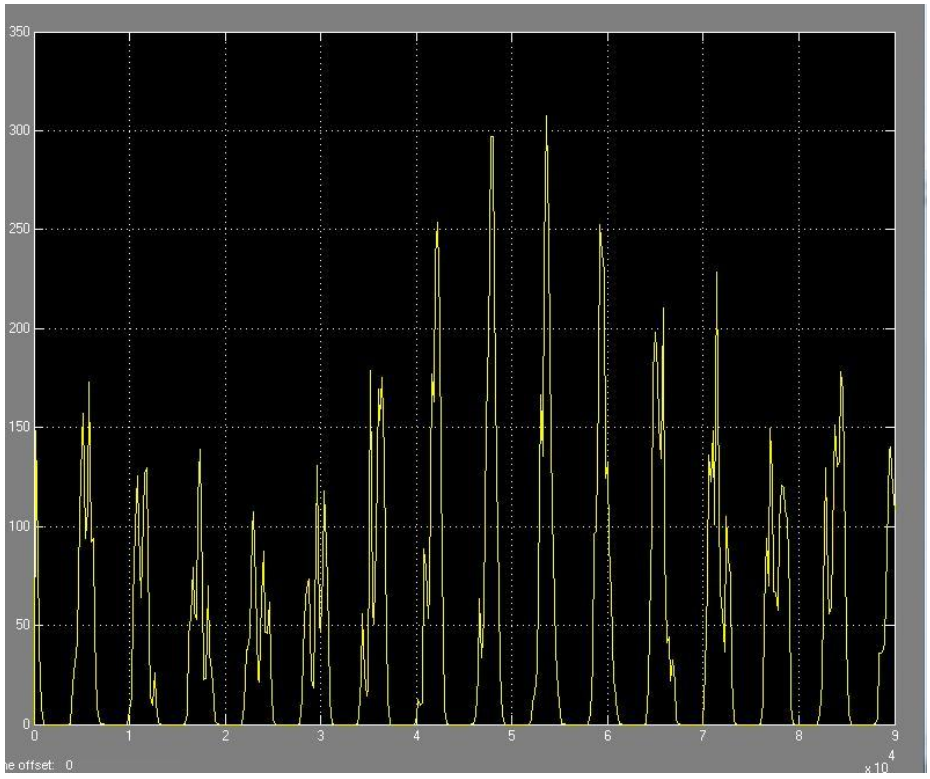

Figure 13: Albedo on the face B'

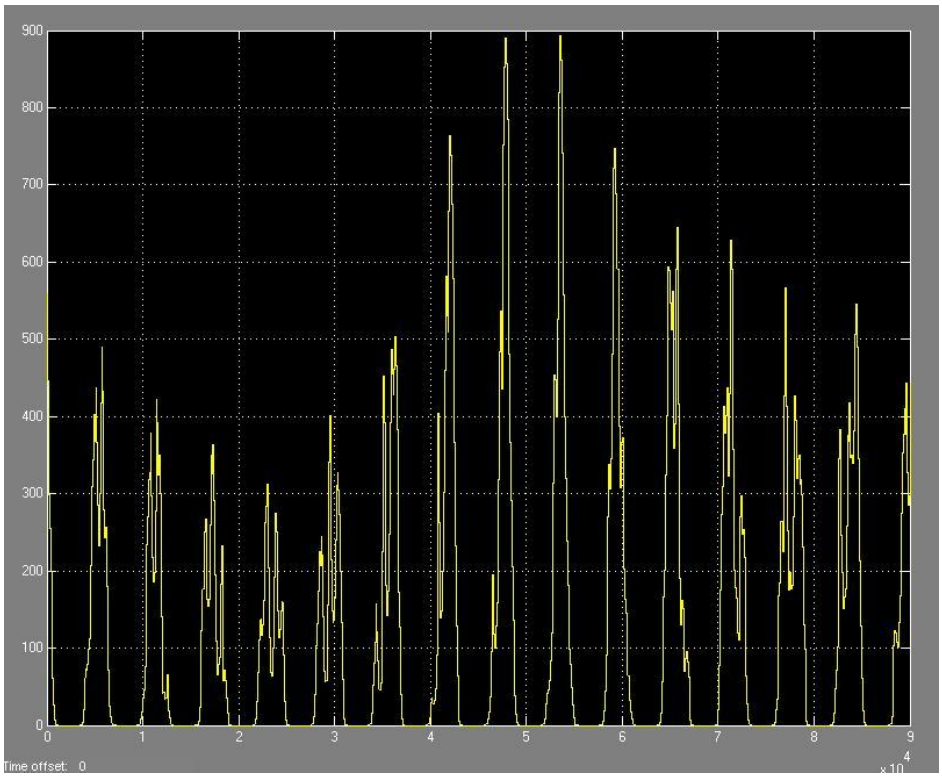

Figure 14: Albedo on face A'

Of particular interest is the daily average albedo incident on each face and the power it generates. This was calculated by the last block in the model.

Face	Daily average albedo
C	40.1 W/m^2
C'	29.8 W/m^2
B	31.8 W/m^2
B'	38.6 W/m^2
A'	122.4 W/m^2
A	0 W/m^2

The face A never faces the Earth. Hence the albedo on it is zero always.

2.2.5 Power due to Earth's thermal radiation

The Earth radiates most of its energy in the band from 5 μm to 100 μm as seen from the following figure. (Source: www.physicalgeography.net)

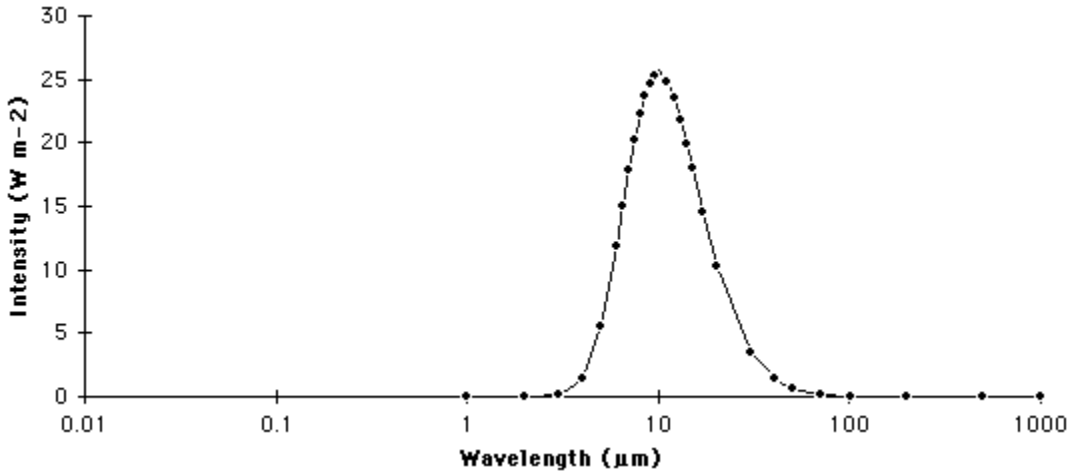

Figure 15: Earth's thermal radiation spectrum

The quantum efficiencies of the three junctions of TJ (Triple Junction) and ATJ (Advanced Triple Junction) solar cells manufactured by Emcore are shown below. (Source: www.emcore.com)

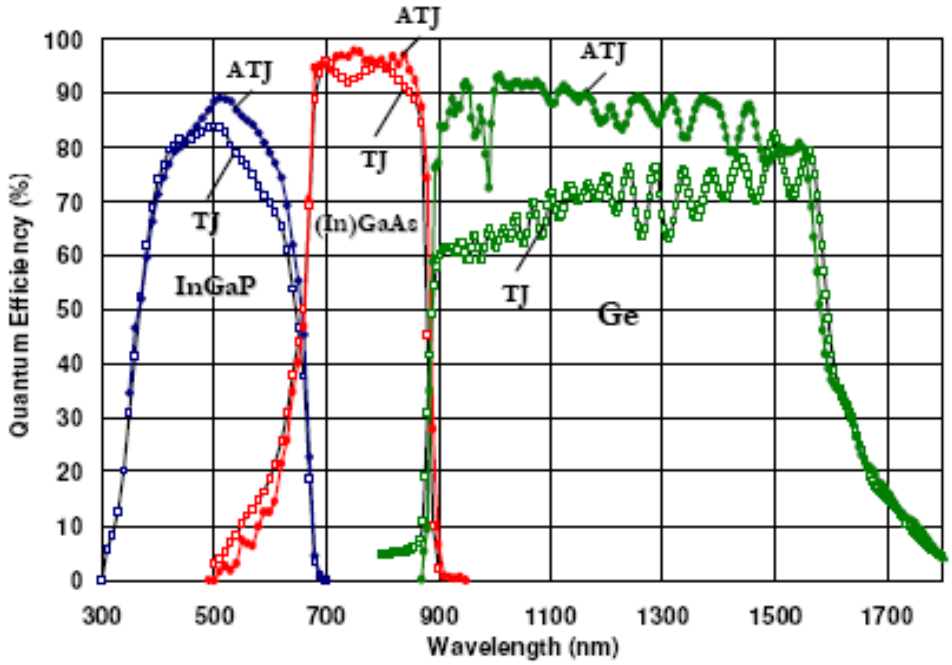

Figure 16: Quantum efficiency of ATJ cell

Thus, the solar cells absorb in a wavelength range of 0.3 μm to 1.8 μm. This shows that the cells cannot absorb any useful radiation from the thermal radiation spectrum of Earth which means that Earth's radiation cannot provide any electrical power to the satellite.

3. Space Radiation Dose

Space environment consists of charged particles such as electrons and protons of varied energies. Their effect on the satellite components can be critical and hence, the components must be simulated and tested for radiation.

3.1 Sources and effects of damaging radiation

The main sources of radiation are the trapped particles in the Earth's magnetic field. Trapped electrons with energies up to 7 MeV and protons with as much as 500 MeV energy are found in the inner Van Allen belts which extend from 700 km to 10,000 km in altitude. As the Earth's magnetic axis is inclined to the rotational axis, the Van Allen belt reach close to 200 km at regions over the South Atlantic Ocean. This effect, called the South Atlantic Anomaly, is a potential source of radiation dose for our satellite. Other high energy particles like neutrons, alpha particles, and UV, X-ray and gamma radiation also cause unpredictable operation of space electronics and degradation of their electrical parameters over time.

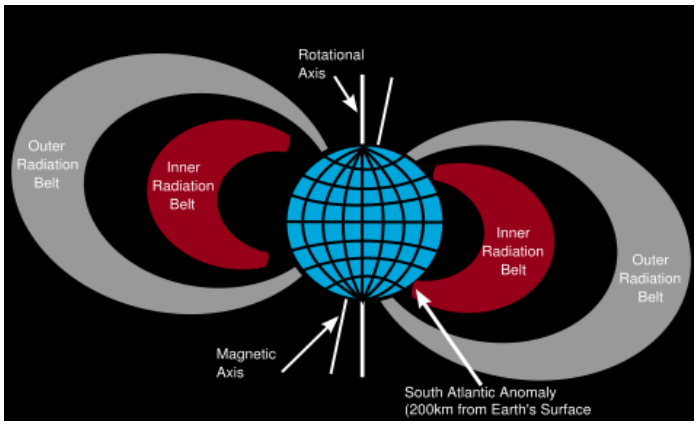

Figure 17: Van Allen belts. Courtesy: Wikipedia

Radiation is measured in two units: neutrons/cm^2 and radiation absorbed dose (rad). The first one is the amount of radiation dose equivalent to an exposure to a collimated beam of a specified number of neutrons per square centimeter having energy of 1 MeV while the second one is the amount of radiation dose causing 0.01J energy to be absorbed by 1kg of the specified matter.

The effects of damaging radiation can be classified as displacement damage and ionization damage. Another type of effect is related to the rate at which radiation is absorbed by the circuits. These include single event effects (SEE) like latch up, bit flips, burn out and snap back caused by a high energy particle creating a trail of ionization inside the bulk of the semiconductor.

Bipolar devices are usually susceptible to displacement damage while ionization damage is more pronounced in MOSFET devices. Most of the electronic devices suffer from single event effects due to the high energies of the incident particles. While special fabrication technologies are required to make radiation hardened ICs, it is possible to design commercial circuits such that the effect of radiation is reduced.

3.2 Simulations

Simulations for effects of radiation on the satellite have been carried out using SPENVIS, the Space Environment Information System by ESA. It is a WWW interface to models of the space environment and its effects. SPENVIS requires a specified orbit to calculate the effects of space weather on it. The following orbit parameters have been used for further simulations –

a. Orbit type: heliosynchronous

b. Eccentricity: 0.00

c. Semi major axis: 7048.16 km

d. Local time on earth at satellite's nadir: 10.30

e. Inclination: 98.07°

f. Period: 1.64 hrs

g. Mission duration: 365.00 days (1.00 years)

Various models have been implemented in SPENVIS for simulating the trapped protons and electrons and their effects for a particular orbit. The entire simulation procedure can be split into the following steps:

3.1 Trapped electrons and protons

3.2 Damage equivalent fluences for solar cells

3.3 Ionising doses

3.2.1 Trapped electrons and protons

The Air Force Research Laboratory (AFRL) (www.vs.afrl.af.mil) has developed two models for the trapped proton and trapped electron environments as seen by the CRRES satellite: CRRESPRO [*Meffert and Gussenhoven*, 1994] for protons, and CRRESELE [*Brautigam and Bell*, 1995] for electrons, respectively. These models are available from the authors, and have been included in AFRL's GEOSPACE software package. With permission from AFRL, the flux maps for these models have been included in the SPENVIS trapped radiation tool, in the framework of the ESA/ESTEC sponsored TREND (TRapped Radiation ENvironment Development) project. These are the latest models for trapped electrons and protons implemented in SPENVIS. These models were used to simulate the trapped radiation under two different conditions-

Quiet solar behaviour: The peak proton flux above 10 MeV came out to be 1.19×10^4 protons per sq.cm. per second. The peak electron flux above 3 MeV came out to be 1.02×10^1 electrons per sq.cm. per second.

Active solar behaviour: The peak proton flux above 10 MeV came out to be 1.05×10^4 protons per sq.cm. per second. The peak electron flux above 3 MeV came out to be 2.85×10^4 electrons per sq.cm. per second.

3.2.2 Damage equivalent fluences for solar cells

The EQFLUX program, developed by the Jet Propulsion Laboratory (JPL) calculate 1 MeV and 10 MeV damage equivalent electron and proton fluences, respectively, for exposure to the fluences predicted by the trapped radiation and solar proton models, for a specified duration. These fluences can then be simulated in the laboratory environment.

The simulations were carried out for the Spectrolab 3J multijunction cells. The radiation models used for electron and proton fluences were the same as in section 3.1 of this document. Assuming no cover glass over the solar cells, the 1 MeV equivalent electron fluences incident on the solar panels per sq. cm. of exposed area over one year were-

a. Quiet solar behaviour - 2.56×10^{14}

b. Active solar behaviour - 3.22×10^{14}

For this radiation, the Spectrolab Triple Junction (TJ) solar cell suffers a degradation of 8%.

3.2.3 Ionising Dose

SHIELDOSE [*Seltzer*, 1980] is a computer code for space-shielding radiation dose calculations. It determines the absorbed dose as a function of depth in aluminium shielding material of spacecraft, given the electron and proton fluences encountered in orbit. SHIELDOSE-2 [*Seltzer*, 1994] differs from SHIELDOSE mainly in that it contains new cross sections and supports several new detector materials, and has a better treatment of proton nuclear interactions.

The radiation models used for electron and proton fluences were the same as in section 3.1 of this document. The thickness of finite aluminium slab shielding the components inside the satellite was assumed to be 2 mm. The following total ionising doses over the period of one year were obtained from the SHIELDOSE-2 model-

a. Quiet solar behavior - 0.718 Krad

b. Active solar behavior – 30.93 Krad

It is of importance to note that most commercial-grade electronics frequently survives up to 30 Krad with or without degradation in performance. Currently, efforts are being taken to understand the simulation of single event effects.

3.3 Choosing components

Most commercial components can be expected to perform without significant degradation during the designed lifetime of the satellite. However, some general rules and tips can be considered such as:

1. Use tested components (components with space heritage) or components made on same assembly line as tested ones
2. Use ROM for storing data.
3. For power MOSFETs, use rad-hard parts or keep generous margins
4. Run microcontroller at less than rated frequency
5. Use shielding (aluminum, tantalum, high-Z metals)
6. Redundancy (not useful for all technologies)
7. Robust electronic design. High drive currents, low fan-out or loading. Large gain margins, high noise immunity
8. Fault tolerant design
9. Error detection and correction
10. Ensure that system can reboot autonomously (watchdog)
11. Database of radiation testing. e.g. Comrad-UK
12. Use same Lot-Date code for test and flight hardware
13. Get components list reviewed by radiation expert (e.g. BARC, TIFR, ISRO scientists)
14. Some commercial ICs are inherently tolerant to radiation. eg. TTL logic, diodes, microwave devices, crystals and most passives

4. Maximum Power Point Tracking of Solar Panels

Maximum power point tracking involves actively varying the voltage and current of the solar panel so as to draw maximum power from them.

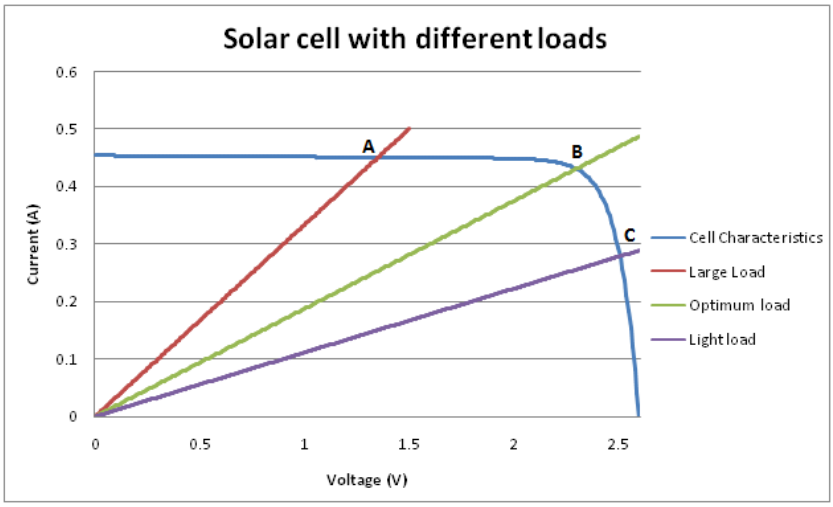

Figure 18: Solar cell with different loads at constant illumination

When a solar cell is connected to a load, the circuit operates at the point common to the cell and load characteristics. In the above figure, the I-V characteristics of a solar cell (at constant illumination and temperature) are plotted along with the characteristics of three resistive loads. When the load resistance is small (i.e. load is large), the circuit operates at point A which results in lower power as the voltage is small. Similarly, with a light load, the circuit operates at point B where the current is low. At the optimum point of operation B, maximum power can be extracted from the cell. This can be seen following graph of the power generated by the solar cell versus its operating voltage.

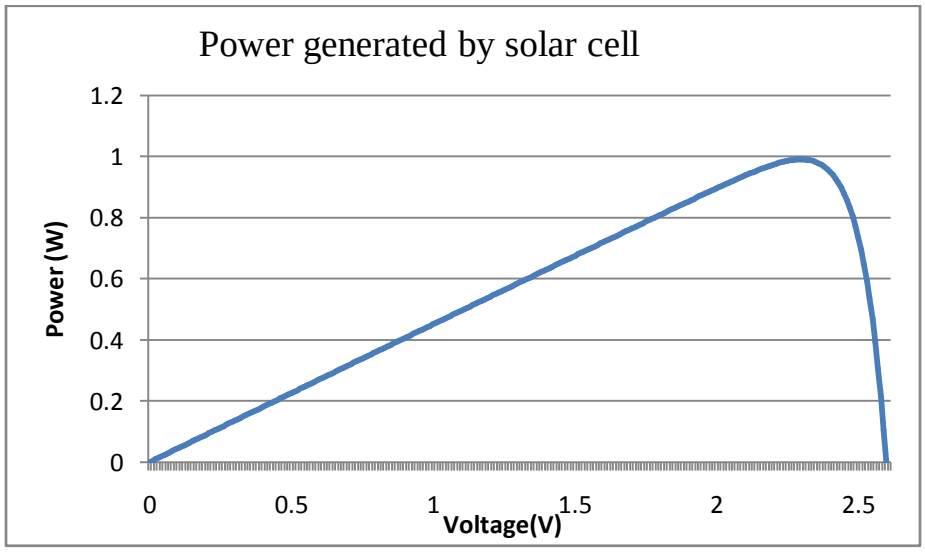

Figure 19: power generated by solar cell at constant illumination

Thus, the objective of MPPT circuit is to ensure that the solar cell always operates at the point of maximum power. This maximum power point (MPP) shifts with varying illumination and temperature of the cell. This variation can be seen in the following P-V graph for a solar cell at different illuminations and temperatures.

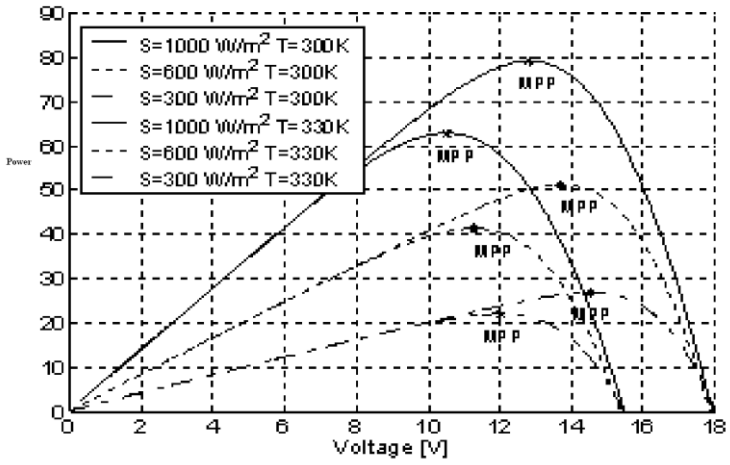

Figure 20: Solar power generated at different illuminations and temperatures

Simple MPPT circuits usually are effective only at a certain operating condition while advanced circuits can achieve tracking of the MPP for all illuminations and temperatures.

4.1 MPPT circuits

The scheme of most MPPT circuits is shown below:

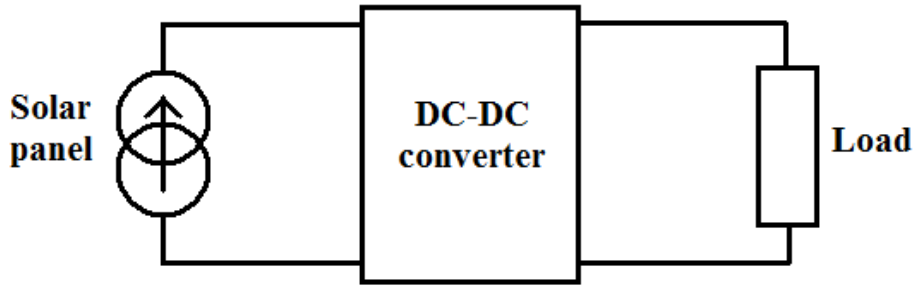

Figure 21: MPPT scheme

The DC-DC converter can be of any type (buck, boost, buck-boost, etc.). But for now, a buck converter is assumed. A typical buck converter looks like this.

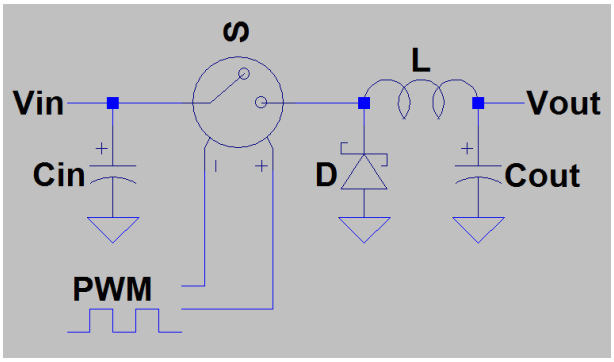

Figure 22: Buck DC-DC converter

The switch, typically a MOSFET, is turned on and off by the pulse width modulated (PWM) signal applied to it. Assuming that current flows through the inductor at all times (continuous conduction mode) and ideal components, the relation between the input and output voltages and currents is as follows:

$$V_{out} = D \cdot V_{in}$$

$$I_{out} = I_{in} / D \quad \text{where D is the duty cycle of the PWM signal}$$

$$\Rightarrow \frac{V_{out}}{I_{out}} = D^2 \cdot \frac{V_{in}}{I_{in}}$$

Thus, the impedance seen by the solar panel (V_{in}/I_{in}) is greater than the load impedance (V_{out}/I_{out}) by a factor of $1/D^2$ (since $0 \leq D \leq 1$). Thus, D can be changed so as to "match" the cell and load impedance, i.e. to ensure that the cell sees the optimum load across itself.

Various methods and algorithms can be used to achieve MPPT. Either an opamp-based circuit or digital control may be used to change D. We considered two methods for MPPT. One is based on a design note by Linear Technology which uses an opamp and voltage reference to change the duty cycle of a buck converter. The other method was to make a simple DC-DC converter and control it using a microcontroller. Both the methods are detailed below.

4.2 Analog MPPT

The analog MPPT circuit is based on a design note by Linear Technology titled "Shrink solar panel size by increasing performance". The circuit diagram is shown below:

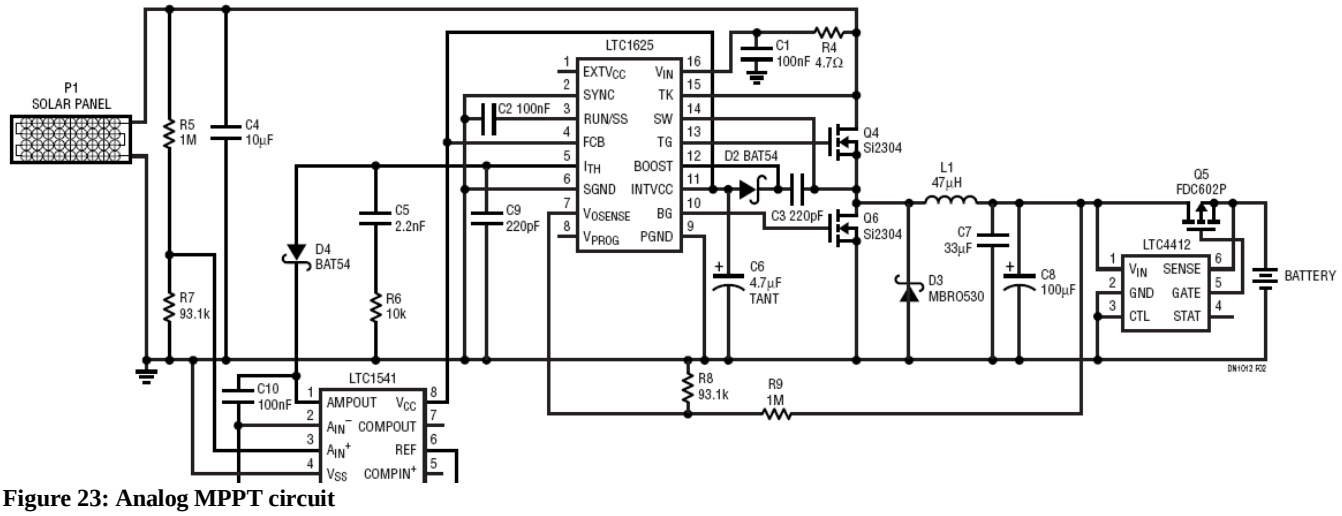

Figure 23: Analog MPPT circuit

4.2.1 Circuit explanation

This circuit implements the constant voltage MPPT algorithm i.e. it tries to keep the solar panel voltage constant throughout the charging. Thus, MPPT is achieved by trying to keep the solar panel voltage close to the voltage which results in maximum power being drawn from it. LTC1625 also tries to regulate its output voltage. The regulated voltage is set to the battery's end-of-charge voltage. Thus, the battery charging is stopped when its end-of-charge voltage is reached.

The above circuit can be broken into three parts: a DC-DC converter, an analog feedback loop, and an ideal diode. The DC-DC converter steps the solar panel voltage down to the battery voltage. The analog feedback loop tries to change the output current so as to maintain a constant solar panel voltage. The ideal diode allows current to flow from the charger to the battery only, thus preventing battery discharge when the solar panel has no light falling on it.

The DC-DC converter is based on the IC LTC1625 which is a constant frequency (150KHz), current mode controller for synchronous step down switching regulator. In a synchronous converter, the top MOSFET acts as the switch as in the buck converter, while the bottom MOSFET is used to reduce the losses in the diode. The IC measures the inductor current by sensing the drain-source voltage of the two MOSFETs. The top MOSFET is turned on at the beginning of every clock cycle and turned off when the inductor current reaches a threshold value. While the top MOSFET is turned off, the bottom MOSFET is turned on until either the inductor current reverses or the next cycle begins. The output voltage is fed back and compared with a reference by an error amplifier. The output of the error amplifier, which is seen on the I_{TH} pin of the IC, changes the inductor current limit to maintain regulation. When the load current increases, it causes a drop in the feedback voltage relative to the reference. The I_{TH} voltage then rises until the average inductor current again matches the load current.

The IC LTC1541 contains an opamp, a comparator and a voltage reference. In this circuit, only the opamp and voltage reference are used.

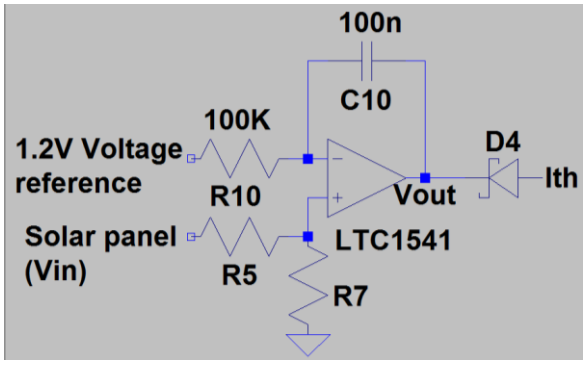

Figure 24: PI control for MPPT

The transfer function for the circuit is: $V_{OUT} = \frac{V_{IN} R_7}{R_5 + R_7} + \frac{1}{R_{10} C_{10}} \int \left(\frac{V_{IN} R_7}{R_5 + R_7} - 1.2 \right) dt$. Due to the diode D_4, the voltage on the I_{TH} pin is clipped to V_{OUT} + diode drop. Thus, when the solar panel voltage rises, I_{TH} voltage increases, which increases the output current, in turn, increasing the solar panel current, which decreases the panel voltage. The solar panel voltage finally stabilizes to $V_{IN} = 1.2\left(1 + \frac{R5}{R7}\right)$.

The ideal diode controller LTC4412 uses an external p-channel MOSFET which is switched on and off depending on whether the diode is to conduct or to cut-off.

4.2.2 Simulation

The above circuit is optimized for a 12V battery (with a 14V end-of-charge voltage) and a 12V solar panel (with 14V maximum power point voltage).The corresponding formulae are:

$$Vmp = 1.2\left(1 + \frac{R5}{R7}\right)$$

$$V_{EOC} = 1.19\left(1 + \frac{R9}{R8}\right)$$

The circuit was modified considering the components available with us.

1) Solar panel: The silicon solar panel we bought has the following characteristics: Voc = 21.3V, Vmp = 17.3V, Isc = 650mA and Imp = 580mA. Considering this, the solar panel model was created.

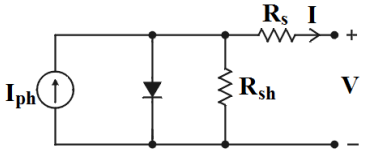

Figure 25: Solar cell model

It shows the following V-I characteristics:

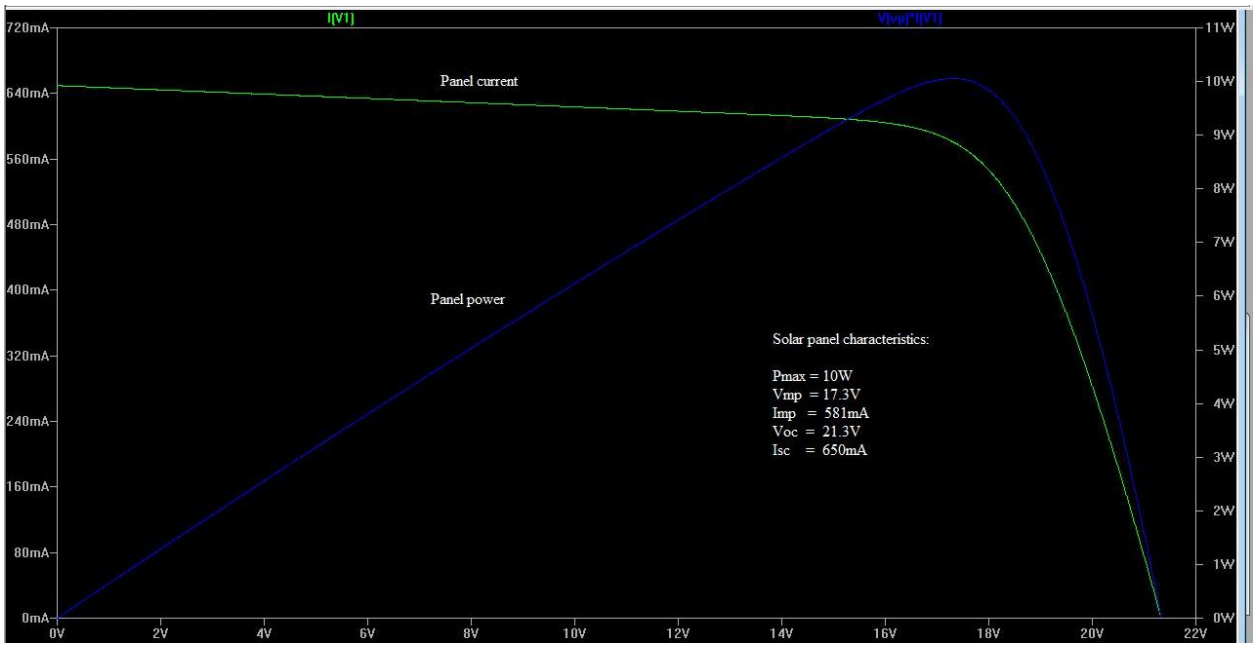

Figure 26: Solar cell simulated characteristics

2) Battery: A 12V lead acid battery with 14V end-of-charge voltage was used.
3) Inductor: The inductor value was changed from 47uh to 33uH.

The final simulated circuit is:

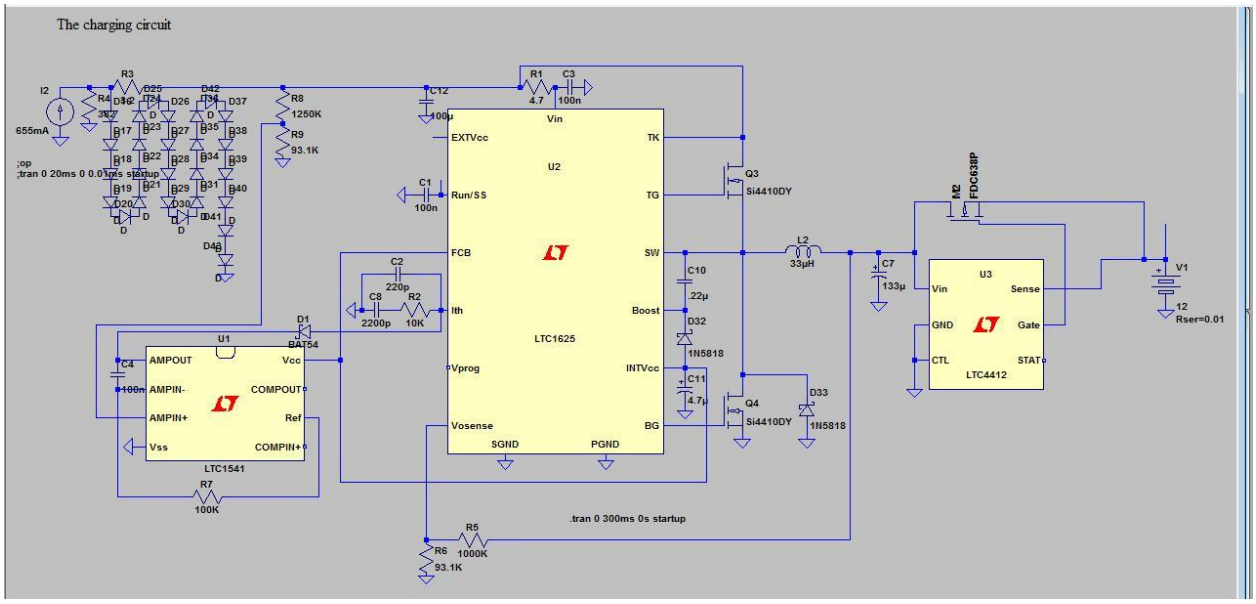

Figure 27: The simulated circuit

The simulation software used is LTspice/Switcher CAD III which is available for free download from the Linear Technology website (www.linear.com). It contains models of the three ICs and other components like MOSFETs, inductors and capacitors commonly used in

switching circuits. It was preferred over the standard simulators after consulting a PG student, Mr. Rohit Modak, VLSI lab, who has experience with the other simulators as well as LTspice.

The simulation results are:

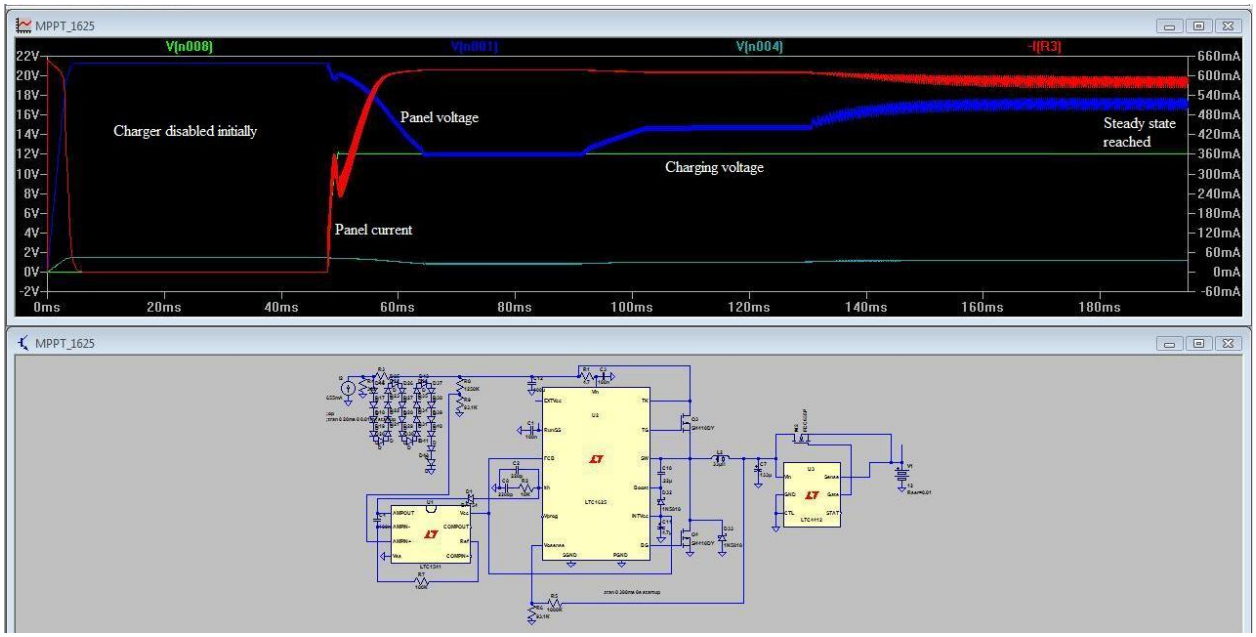

Figure 28: Complete analog MPPT circuit behavior

As we can see, the solar panel voltage stabilizes to its maximum power point voltage within 200 milliseconds. A close-up of the steady state is shown.

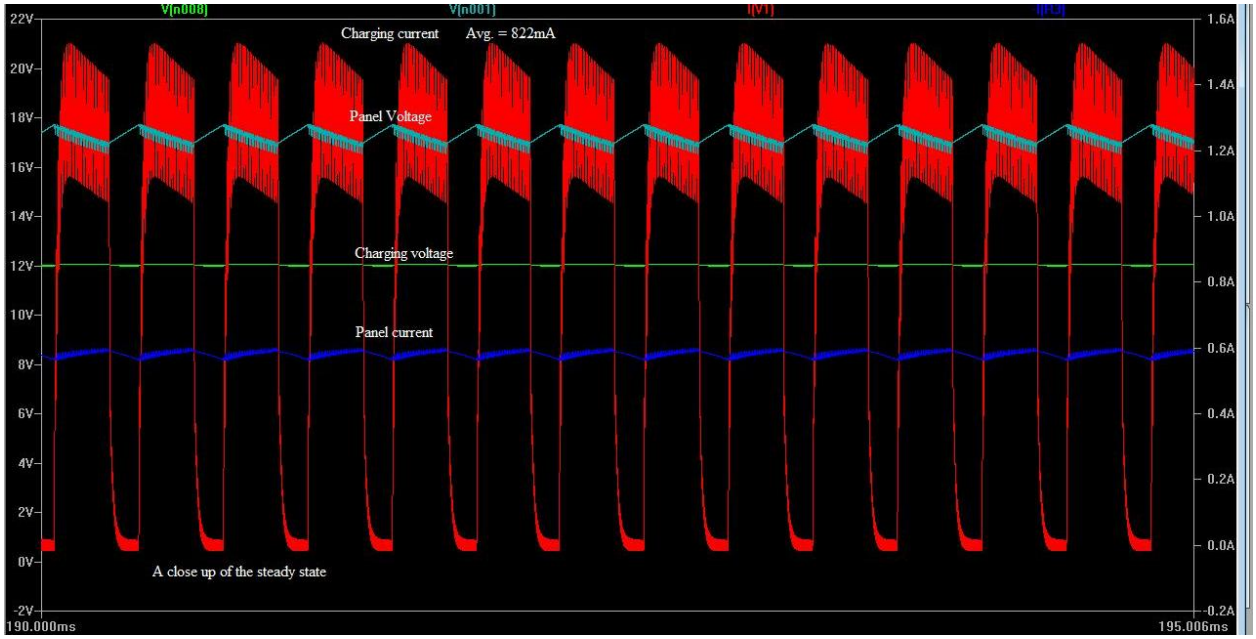

Figure 29: The steady state close up

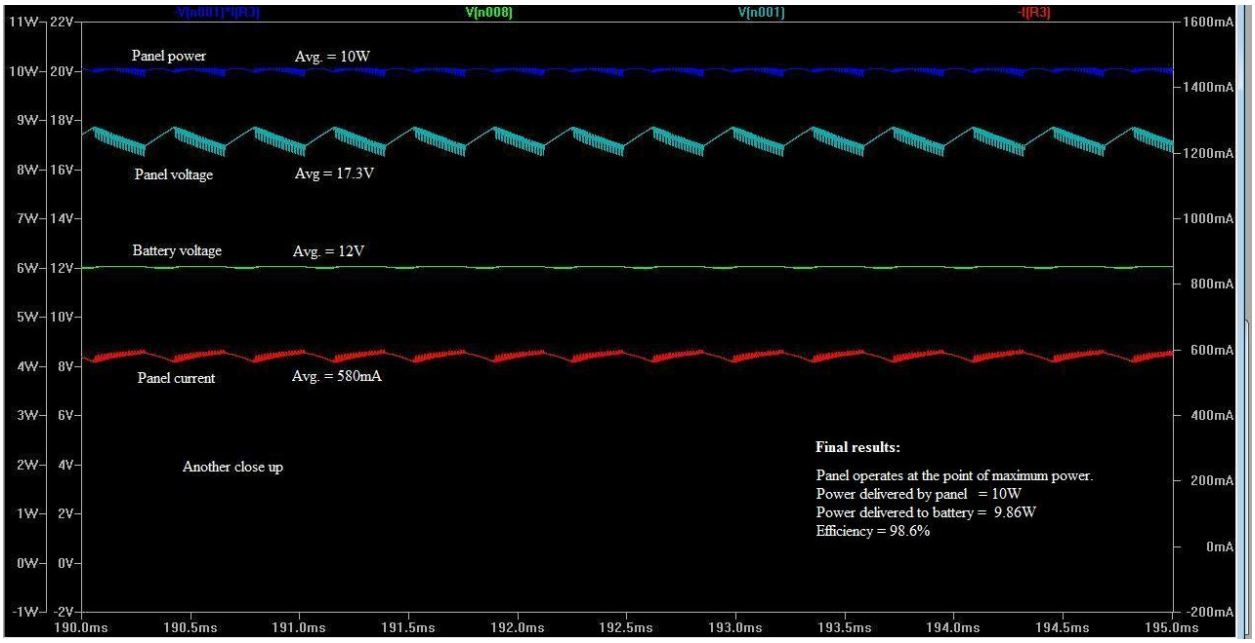

Figure 30: The steady state close up

The final results are:

1. Panel operates at the expected point at which it is set.
2. Power delivered by the solar panel = 10W
3. Power delivered to the battery = 9.86W
4. Hence, total efficiency of the MPPT algorithm and DC-DC converter = 98.6%

The efficiency obtained is unrealistically high as some components were considered ideal. Also, effects of pcb layout which are noticeable at the switching frequency of 150KHz cannot be simulated by the simulator.

4.2.3 Testing

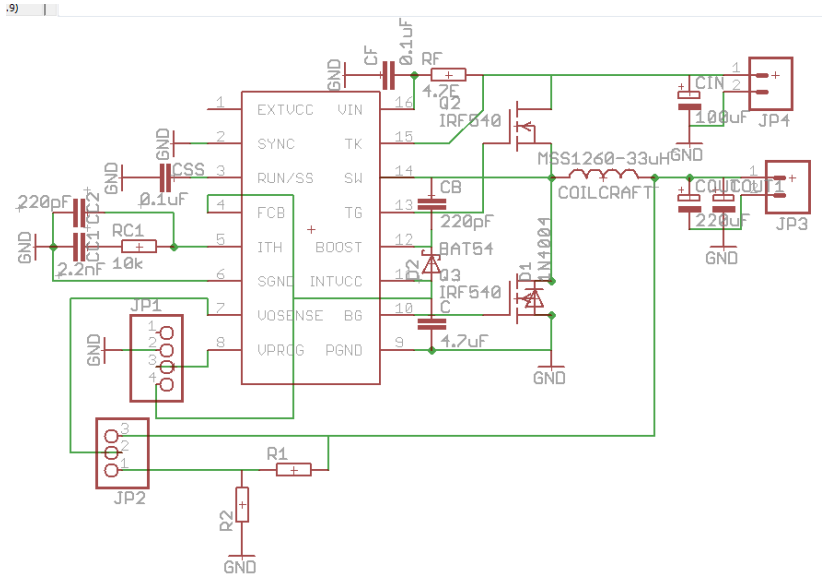

Figure 31: Schematic of circuit assembled

The above circuit was assembled on a PCB made from PCB lab, EE department. The individual parts of the circuit i.e. the DC-DC converter, opamp and the ideal diode were separately tested. The DC-DC converter was given 10V input voltage. The output voltage was set to 3.3V, 5V and 7.8V and output power was up to 5W. The DC-DC converter showed efficiencies between 85% and 90%. The ideal diode had a forward drop of 0.05V. However, when the three circuits were put together, the circuit did not work. The problem was found to repeatedly occur when the output of the opamp was connected to the I_{TH} pin.

4.3 Digital MPPT

In digital MPPT, a microcontroller is used to change the duty-cycle of the PWM signal given to the DC-DC controller using feedback from the input and output voltages and currents. Since, changing the MPPT algorithm involves a simple change of the microcontroller program, this MPPT implementation is much more flexible than the analog method. The downside is that the switching frequency is somewhat lower.

An ATmega16 microcontroller was used for testing as we have prior experience in using it. The microcontroller has 16KB of flash memory, 1KB of SRAM and can run upto 16MIPS with a 16MHz clock. It has various peripherals like serial communication (UART) and 8-channel 10-bit analog to digital converter (ADC) which proved useful in the circuit. The DC-DC converter was built with an input current sensor on a prototyping board. The circuit diagram is shown below.

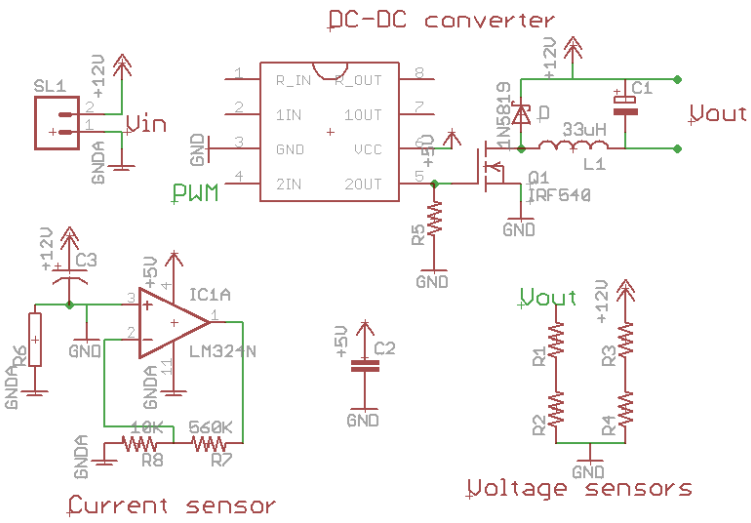

Figure 32: Schematic of circuit assembled

A 20 ohm 10W resistor was used as a load for a 17.3V 0.58A (maximum power AM0) solar panel. The switching frequency is 62.5 KHz. The duty cycle was varied from 0 to 1 and the output voltage, input voltage and current were logged to a computer using the serial interface. The following results were obtained on June 5, 2008 at 12 noon.

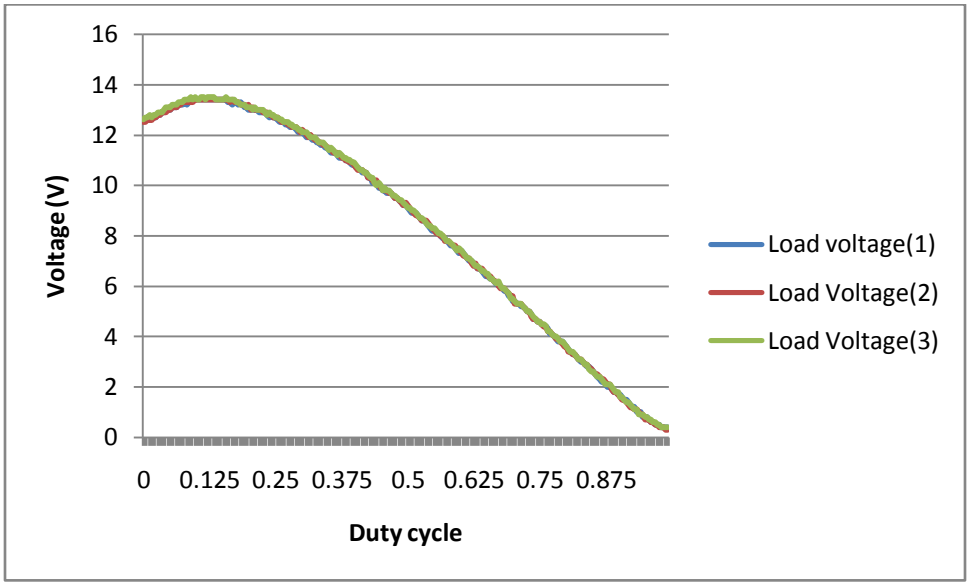

Figure 33: MPPT results

Thus, we can see a clear point of maximum power. Various algorithms were tested out such as constant input voltage, maximum output voltage and perturb and observe. The codes were written in C and compiled using AVR-GCC. All of them were found to reach the maximum power point successfully.

5. Flight Hardware and Software

We now describe the hardware to be used on the satellite.

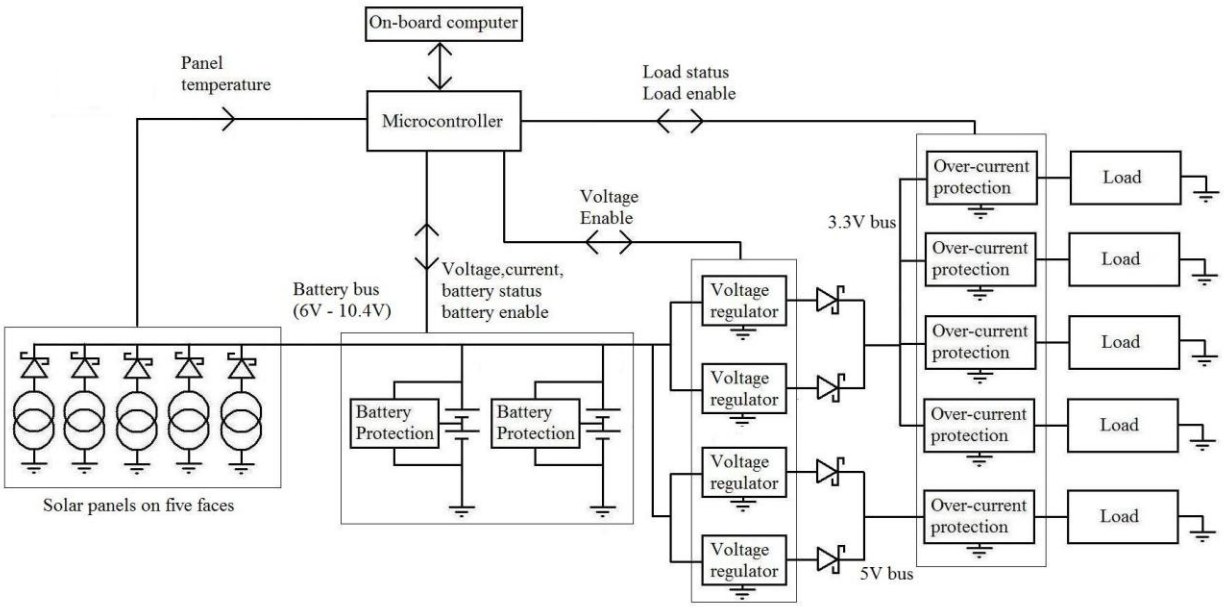

Figure 34: Flight hardware

Five solar panels with reverse blocking diodes are connected to the battery bus. The batteries are connected in a 2-series 2-parallel configuration for redundancy and have protection circuits on them. Voltage regulators step down the battery voltage to 5V and 3.3V. There are current limiting switches in series with each load to ensure shut-down in case of excessive power drawn by that particular load.

5.1 Solar cells and panels

The satellite is powered by solar panels on five faces. One of the side faces is reserved for the antennae and the launch vehicle interface; so there is no solar panel mounted on that face.

Advanced Triple Junction (ATJ) cells from Emcore have been decided for the satellite. The cells have been chosen considering their flight heritage, high efficiency and resistance to radiation. We will buy the cells in the CIC (covered cell interconnect) form and they will be assembled in a panel at the solar panel lab facility at ISAC. The beginning-of-life specifications of the ATJ cells at air-mass 0 spectrum (1353W/m^2) and 28 ^oC are:

- V_{OC} = 2.60 V
- V_{MP} = 2.30 V
- J_{SC} = 17.1 mA/cm^2
- J_{MP} = 16.20 mA/cm^2
- Maximum efficiency = 28.5%

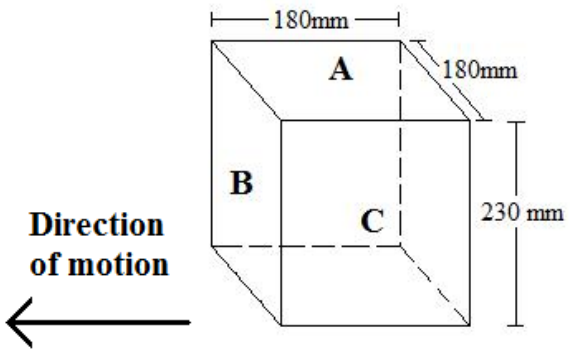

Figure 35: Satellite motion

- Fill-factor = 0.84

The faces A and A' have 8 cells each and the faces B, B' and C have 12 cells each. All faces have the cells connected in strings of four cells in series. Hence, faces A and A' have 2 such strings while the other faces have 3 such strings. Since no sunlight ever falls on the face C', that face has been used for the antennae and the launch vehicle interface.

Thus, the voltage ratings of all the panels are the same: V_{OC} = 10.4V and V_{MP} = 9.2V.The maximum temperature of the solar panels is calculated by the thermals team to be around 35° C. Hence we shall assume room temperature values for all subsequent calculations.

5.2 Battery pack

Rechargeable lithium-ion technology has been selected for the satellite considering their superior performance and characteristics over the other battery technologies like nickel cadmium (NiCd) and nickel metal hydride (NiMH). The cells will be purchased from 'Saft batteries' which has experience in space grade batteries. The cell MPS 176065 has the following characteristics:

Guaranteed capacity	5.8 Ah
Mean voltage at C/1.5	3.6 V
End of charge voltage	4.1 V
Energy	20 Wh
Specific energy	133 Wh/kg
Dimensions	65mm x 65 mm x 18mm
Weight	0.15kg

They will be assembled into a 2-series 2-parallel pack. Thus, the total rating of the battery is:

- Mean voltage = 7.2V
- Guaranteed capacity = 11.6 Ah
- Energy = 80Wh
- Depth of discharge = 6%
- For a power consumption of around 10W, the satellite can run for around 8 hours without solar power on a full battery.

The battery specifications can be seen in detail in the following figures.

Technology	Capacity	Weight	Mass energy density	Energy	Internal resistance
	[Ah]	[g]	[Wh/kg]	[Wh]	[mΩ]
Cobalt	5,6	151	132,5	20,0	45

Table 2. Insured MP176065 electrical performances @20°C

The graph hereunder indicates MP 176065 cell electrical performances for discharges performed at 20°C under different rates from C/5 to 3C.

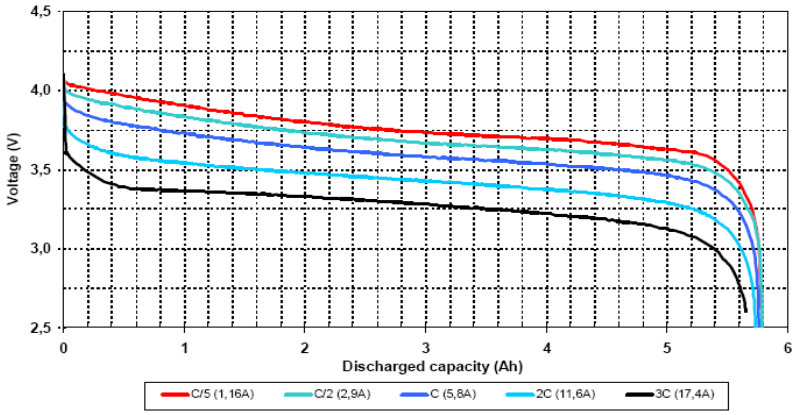

Figure 3. Capacity versus discharge current for MP176065 cell, BOL @ 20°C.

Figure 36: Battery characteristics

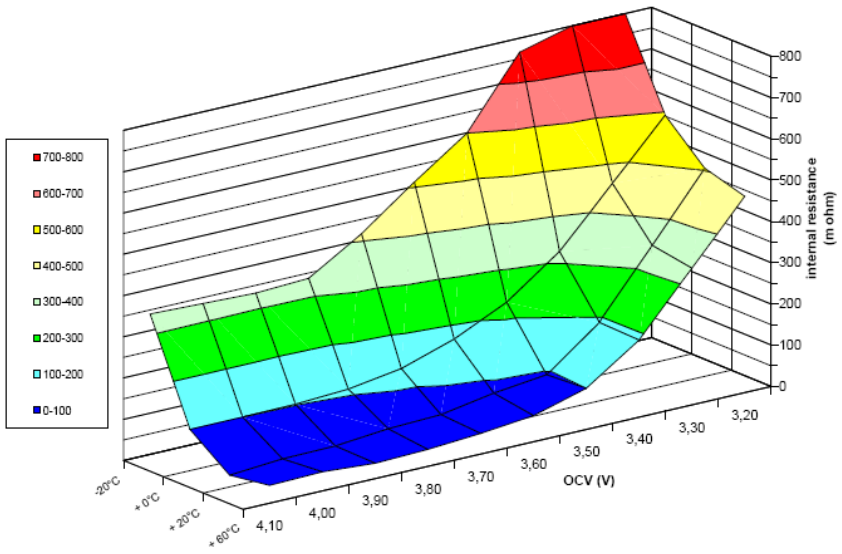

Figure 37: Battery characteristics

The variation of internal resistance of the cell with temperature and open circuit voltage is seen in the above 3-D plot. This shows the useful temperature range of the battery to lie between 0°C and 60°C. For safety purposes, it is best to operate the cells within 20°C and 40°C.

5.3 Battery charge regulation and protection

The ideal charging method for Li-ion batteries is a constant-current, constant-voltage (CCCV) charging algorithm. In this method, the battery is charged with a constant current (usually 1C) until the voltage reaches the end-of-charge (EOC) voltage. Once the EOC voltage is reached, the charger switches to a constant voltage charging where the charging current automatically falls with time. The battery is declared "charged" when the charging current drops to a predetermined limit.

On the satellite, the maximum charging current ever available is much smaller than 1C. Also, the varying sunlight intensity makes it impossible to maintain the CCCV algorithm always. Hence, it was decided not to use any dedicated battery charger IC but to use a combination of the microcontroller and the battery protection IC for regulating the battery charging.

Battery protection ICs from Texas Instruments and Seiko Instruments are being considered for the satellite. All these ICs incorporate overcharge, over discharge and overcurrent protection for two Li-ion or Li-polymer cells with the use of series FETs to allow and prevent the connection of the battery with the battery bus. The UCC3911-x (x = 1,2,3,4) from TI has internal FETs and has been used by AAUSAT before. However, the IC has overvoltage protection thresholds which are suitable for Li-ion cells with an EOC voltage of 4.2V. Hence, it cannot provide overvoltage protection to the SAFT battery. The ICs from Seiko have a large range of overvoltage thresholds and some ICs are found suitable for our battery. However, these ICs require external MOSFETs and their performance in space is unknown. The UCC3911 also provides status outputs like undervoltage, overvoltage and low power warning and also an enable pin which make them easier to work with than the Seiko products.

The specifications of S-8232 (from Seiko Instruments) are as follows:

- Internal high-accuracy voltage detection circuit
- Overcharge detection voltage: 3.85 V ± 25 mV to 4.60 V ± 25 mV in 5 mV step
- Overcharge release voltage: 3.60 V ± 50 mV to 4.60 V ± 50 mV in 5 mV step
- Overdischarge detection voltage: 1.70 V ± 80 mV to 2.60 V ± 80 mV in 50 mV step
- Overdischarge release voltage: 1.70 V ± 100 mV to 3.80 V ± 100 mV in 50 mV step
- Overcurrent detection voltage: 1 0.07 V ± 20 mV to 0.30 V ± 20 mV in 5 mV step
- High input-voltage device: Absolute maximum ratings 18 V.
- Wide operating voltage range: 2 to 16 V
- The delay time for all detections can be set via an external capacitor.
- Two overcurrent detection levels (Protection for short-circuiting)
- Internal auxiliary over voltage detection circuit (Fail-safe for overcharge detection voltage)
- Internal charge circuit for 0 V battery (Unavailable is option)
- Low current consumption

- Operation mode 7.5 μA typ. 14.2 μA max. (–40 to + 85 °C)
- Power-down mode 0.2 nA typ. 0.1 μA max. (–40 to + 85 °C)

The specifications for UCC3911-x are:

- Protects Sensitive Lithium-Ion and Lithium-Polymer cells from overcharging and overdischarging
- Used for two-cell battery packs
- No external FETs required
- Provides protection against battery pack
- Output short circuit
- Extremely low power drain on batteries of about 20 μA
- Low internal FET switch voltage drop
- User controllable delay for tripping short-circuit current protector
- 3-A Current Capacity

state transition threshold

PARAMETER			TEST CONDITIONS	MIN	TYP	MAX	UNITS
V_{OV}	Overvoltage threshold	UCC3911–1		4.15	4.20	4.25	V
V_{OVR}	Overvoltage threshold recovery			3.60	3.70	3.80	
V_{OV}	Overvoltage threshold	UCC3911–2		4.20	4.25	4.30	
V_{OVR}	Overvoltage threshold recovery			3.65	3.75	3.85	
V_{OV}	Overvoltage threshold	UCC3911–3		4.25	4.30	4.35	
V_{OVR}	Overvoltage threshold recovery			3.70	3.80	3.90	
V_{OV}	Overvoltage threshold	UCC3911–4		4.30	4.35	4.40	
V_{OVR}	Overvoltage threshold recovery			3.75	3.85	3.95	
V_{UV}	Undervoltage threshold			2.42	2.50	2.58	
V_{UVR}	Undervoltage threshold recovery			2.90	3.00	3.10	

The battery protection IC can take care of all the fault cases independent of the microcontroller. However, the microcontroller may also be used to monitor the battery voltage and prevent overcharging and overdischarging. This will require the use of MOSFET switches to control the flow of power as and when the fault conditions are reached.

5.4 Total power available

For the loads mentioned in the first chapter and a 30 minute eclipse time, we find that the depth of discharge of the battery is 6%. This means that if the battery is fully charged at the beginning, its voltage will always lie between 8V and 8.2V. Assuming a forward drop of 0.3V for the schottky diodes, the current supplied by each panel was calculated. The average power was found to be approximately 11W. With the use of a dedicated MPPT circuit, this value was found to increase up to 13W only. The total power loss in the power distribution circuit was

found to be 1.5W. Hence the total power requirement is 7.1W, which leaves us with an excess of about 4W in the power budget.

5.5 Voltage regulators

The voltage regulator (also known as the power conditioning module) converts the raw battery or solar panel voltage into a regulated voltage for the loads. An industrial grade DC- DC converter will be used considering following factors:

1) Output voltage(s) : 3.3V, 5V
2) Input voltage range : 5-10 Volts
3) Typical and maximum output current
4) Switching frequency
5) Efficiency (>85%)
6) Output ripple
7) Electromagnetic interference(EMI)
8) Phase margin (stability)
9) Transient response
10) Soft start
11) Standby mode
12) Redundancy

The PTR08060 and PTH08080 step-down switching regulators from Texas Instruments have been selected for this purpose. Two such modules will be paralleled together with cold redundancy. The electrical specifications of PTR08060 are:

- Up to 6A Output Current
- Wide Input Voltage Range (4.5 V to 14 V)
- Wide-Output Voltage Adjust (0.6 V to 5.5 V)
- Efficiencies Up To 96%
- ON/OFF Inhibit
- Undervoltage Lockout (UVLO)
- Output Overcurrent Protection (Nonlatching, Auto-Reset)
- Overtemperature Protection
- Ambient Temp. Range: –40°C to 85°C
- Space Saving Vertical SIP Package

The PTH08080 has the specifications:

- Up to 2.25-A Output Current at 85°C
- 4.5-V to 18-V Input Voltage Range
- Wide-Output Voltage Adjust (0.9 V to 5.5 V)

- Efficiencies Up To 93%
- On/Off Inhibit
- Undervoltage Lockout (UVLO)
- Output Overcurrent Protection (Nonlatching, Auto-Reset)
- Overtemperature Protection
- Ambient Temperature Range: –40°C to 85°C

Consider the loads on the two buses, the PTR08060 is to provide 3.3V and PTH08080 is for 5V. The current limits of the modules leave a wide margin with no loss in efficiency. The wide input voltage range covers the entire useful battery voltage range of 6V to 8.4V.The modules can be switched on and off by the power systems microcontroller through the ON/OFF inhibit pin. The industrial temperature range makes the module suitable for our application.
The application circuit for PTR08060 is shown below. The other module has a similar circuit.

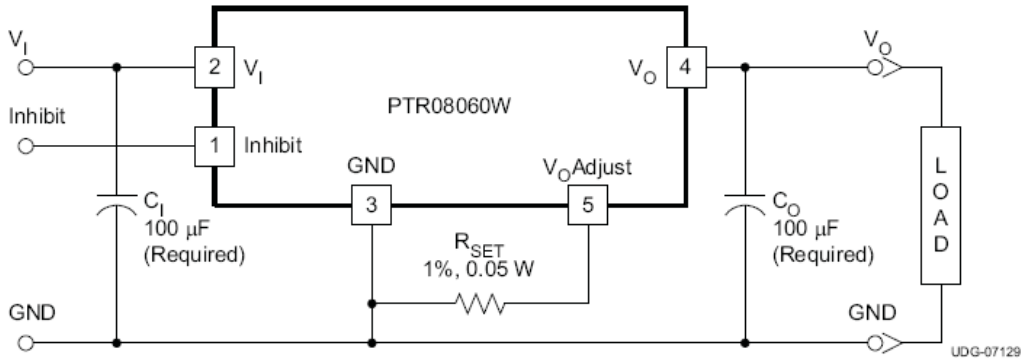

Figure 38: Application circuit for PTR08060

Courtesy: PTR08060 datasheet, Texas Instruments, www.ti.com

Aluminum electrolytic capacitors cannot be used at the input and the output as they are not recommended for use below 0^{o}C. Hence, other type of capacitors like OS-CON, poly-aluminum or polymer-tantalum capacitors will be used as recommended in the datasheet. The actual type of capacitor used will depend upon their availability in the market. The output voltage is set by the R_{SET} resistor. A 432Ω gives an output voltage of 3.327V.

5.6 Current Distribution switches

MOSFET switches of very low internal resistance will be used for power distribution. Considering internal resistance, current capacity & flight heritage, IC tps203x from Texas Instruments was chosen. It has the following features:

- 33-mΩ internal resistance
- Ambient Temperature Range, –40°C to 85°C
- Short-Circuit and Thermal Protection ·
- Overcurrent Logic Output

- Operating Range: 2.7 V to 5.5 V
- Logic-Level Enable Input
- Typical Rise Time: 6.1 ms
- Undervoltage Lockout
- Maximum Standby Supply Current: 10 μA
- No Drain-Source Back-Gate Diode

5.7 Microcontroller

The main functions of the microcontroller are as follows:

- The microcontroller turns on the other circuits a specified amount of time after ejection from the launch vehicle.
- It regulates the charging of the battery.
- It monitors the load status information (normal/overcurrent) provided by the current limiting switches.
- Faulted loads are immediately switched off and OBC is notified.
- Voltage regulators can also be switched off in case of faults and power down.
- Faulted loads are switched ON on periodical command from the OBC.
- Readings for health monitoring are conveyed to the OBC every minute.
- Power microcontroller is powered off the battery bus by a separate linear power supply.

Since using space grade microcontrollers is prohibitively expensive, commercial ones with one-time programmable (OTP) memory will be used. An 8-bit PIC microcontroller has been chosen considering its use in various satellites like Rincosat, Stensat-2 and AAUSAT previously.

A corresponding pin compatible flash memory PIC device for the OTP device will be used to test and build all the circuits. Finally the flash device will be replaced by the OTP device. The PIC16C77 has been chosen as the flight microcontroller for the power system. The testing will be done on a PIC16F877A. The PIC16C77 has the following features:

Microcontroller Core Features:

- High-performance RISC CPU
- Only 35 single word instructions to learn
- All single cycle instructions except for program branches which are two cycle
- Operating speed: DC - 20 MHz clock input DC - 200 ns instruction cycle
- Up to 8K x 14 words of Program Memory, up to 368 x 8 bytes of Data Memory (RAM)
- Interrupt capability
- Eight level deep hardware stack
- Direct, indirect, and relative addressing modes
- Power-on Reset (POR)

- Power-up Timer (PWRT) and Oscillator Start-up Timer (OST)
- Watchdog Timer (WDT) with its own on-chip RC oscillator for reliable operation
- Programmable code-protection
- Power saving SLEEP mode
- Selectable oscillator options
- Low-power, high-speed CMOS EPROM technology
- Fully static design

Program Memory (EPROM) x 14	8K
Data Memory (Bytes) x 8	368
I/O Pins	33
Parallel Slave Port	Yes
Capture/Compare/PWM Modules	2
Timer Modules	3
A/D Channels	8
Serial Communication	SPI/I^2C, USART
In-Circuit Serial Programming	Yes
Brown-out Reset	Yes
Interrupt Sources	12

Figure 39: PIC16F877A features

PIC16f877a has some compatibility issues with the third party programmer we are using, but other microcontrollers of the same family: PIC16F84A and PIC16F628A have been tested. A universal programmer from HI-LO Systems was used for programming the PIC microcontrollers. The programs were written in assembly and compiled using the MPLAB Assembler and Simulator from Microchip. A software called WACCESS transferring the hex files to the microcontroller using the programming hardware.

The PIC16f84a and PIC16f628a were successfully programmed and tested with various codes. The following codes were simulated and tested:

- Timers using software and hardware
- Codes for testing the Low voltage programming (LVP) and High voltage programming (HVP) options. The performance of PIC16f628a with LVP was not satisfactory and PIC16f84a has only HVP.
- Codes involving ADCs were simulated but could not be tested. Neither 16F84a nor 16F628A has ADC facility.

The PIC16f877a was found to have a problem with the system clock. As the same issue was observed on three ICs, there might be some problem with the configuration bit settings set by the programmer.**(***reference: Design with PICMicrocontrollers, John B.Peatman, Pearson Education, page no 9).*Now we have decided to buy a PIC programmer available from Microchip itself.

We have the radiation testing data for the PIC16f877a device. And the corresponding OTP device has similar architecture. This data will be useful as we might not be able to do any actual radiation testing on the devices we have.

5.8 Hardware list

Sr. no.	Component	Description	Nos. used
1.	Solar cells	Emcore ATJ solar cells	52
2.	Batteries	SAFT 3.7V, 5.8Ah	4
3.	3.3V regulator	TI PTR08060, integrated switch-mode regulator	2
4.	5V regulator	TI PTH08080, integrated switch-mode regulator	2
5.	Microcontroller	Microchip PIC16C77	1
6.	Power distribution	TI TPS203x, current limiting switches	TBD
7.	Battery protection	TBD	
8.	Power OR-ing diodes	TBD	
9.	RBF pin, kill and charging switches	TBD	